nature portfolio

Peer Review File

Perovskite–organic tandem solar cells with a photo-transformable stabilizer

Corresponding Author: Professor Lei Meng

Any redactions in this file are there to maintain patient confidentiality, the confidentiality of unpublished data, or to remove third-party material.

Parts of this Peer Review File have been redacted as indicated to remove third-party material.

Attachments originally included by the reviewers as part of their assessment can be found at the end of this file.

Version 0:

Reviewer comments:

Referee #1

(Remarks to the Author)
In this manuscript present a new additive that improves efficiency and stability of wide gap perovskite solar cells and eventually enables impressive perovskite-organic tandem solar cells with an, to the best of my knowledge, unprecedented operation stability with a T90 of over 600h. As of that, I believe that this result is worth reporting and the nature family is a suitable platform for that, considering the enormous potential of perovskite-organic tandem solar cells – especially in the context of stability. Indeed extrapolated the authors stability seems to be almost at par with the current all-perovskite tandem record from Hairen's group (it should be expected to have something of 84% after 1000 hours of stress. I would amend the authors to mention this aspect prominently, as it can motivate others to joint the community and contribute to its success. Another very important aspect is the choice of solar cell calibration. Curiously for some reason, currently the community is moving backwards with respect to reliability especially of multi-junction solar cell data. The Calibration certificate that the authors provide does not contain a measurement of the quantum efficiency, which casts doubt, that the calibration has been performed under properly adjusted light sources (see e.g. 10.1002/solr.202200800). Not following proper measurement protocols, has unfortunately led to a situation, where the progress of the field is currently not reflected in well-accepted collections as the NREL efficiency chart or the Green solar cell efficiency tables. On top of that, the authors are actually stating the reverse scan of the calibration, instead of the stabilized value (which is 27.6%, if I calculated correctly from the certificate). If the main reason for publication of a study is the efficiency, every author has to take extra care, that it is measured correctly. I can only recommend publication on this motivation, if a well accepted calibration protocol is used.

That's also where the trouble begins - while the devices are nature level, the science behind these devices still needs some serious work-over and additional insights – Afterall a scientific paper should not only state a result, but also unravel the underlying mechanisms. From a birds-view perspective, the authors mainly elaborate on the effect of their TDB additive – anyhow towards the mechanism that is actually at play here remains elusive and the discussion remains rather superficial and contains a lot of speculation, that is sometimes in contradictions to recent findings in the field.

Two key topics and key issues here are the crystallization mechanism and the halide segregation topic, that I will address separately here:

Halide segregation:
Here the authors consistently reproduce a common misconception on the origin and damage mechanism of halide segregation, that has been miss-proven for quite a while now. As shown e.g. 10.1021/acsenergylett.0c01104, recombination is actually not the key issue in a halide segregated solar cell – the authors unfortunately only show the development of the PCE data and only fast hysteresis of fresh devices (leaving out Jsc, which I don't understand), but in my experience halide segregation typically strongly impacts on Jsc, as it increases the amount of mobile ions and increases ionic losses (see 10.1038/s41560-024-01487-w). In general the discussion on the topic is relatively thin, taking into account that there has been extensive studies and reviews on halides segregations (one even targeting perovskite-organic tandems e.g. in 10.1038/s41578-023-00642-1) and by the use of e.g. redox shuttles to reintegrate oxidized species (10.1038/s41560-024-

01451-8) there have already been targeted strategies to overcome the root cause of halide segregation. The observed photoactivity of the TDB molecule appears to be interesting, but the mere fact that it sits at the grain boundary is not a mechanism and does not explain, how it is able to reduce the oxidization of iodide or the formation of hole accumulations. The authors should provide an in-depth study on how this molecule can tackle the root cause of halide segregation, taking into account up to date literature on the topic and building from it.

Crystallization:
Here the manuscript similarly shows an incomplete discussion and in part bases their hypothesis on incomplete and outdated hypothesis. One of the key points of argumentation that the authors use to argument the beneficial effect of their TDB molecule is an interaction inside the solution. Now there has been a very recent study demonstrating, that such deductions are not valid, as firstly the interaction in the perovskite precursor solution are highly complex due to the formation of solvates (see e.g. 10.1021/acs.jpclett.0c03741, which the authors don't account for) and, most importantly, secondly largely unrelated to the final crystal formation process (10.1038/s41467-025-65484-7). Actually in-situ GIWAXS studies on mixed halide perovskites (10.1021/acsami.3c18623) straightforward show, that a segregated initial stage is pretty common when depositing wide gap perovskites and the formation of the final mixed perovskite occurs during annealing. Throughout the manuscript the authors argument with "nucleation" of the perovskite and "preferred formation of Br-rich nuclei" etc. without having any way of measuring the process of nucleation, which occurs at the very moment of anti-solvent exposure. A transition from the delta to the alpha phase is certainly not a nucleation process. Also the process of halide mixing during annealing cannot be explained by nucleation. Rather it is a reorganization of the already existing crystal structure, which would most probably involve additive driven grain coarsening (see 10.1038/s41467-025-65484-7). Indeed there is some striking resemblance between this work and the work from Maschwitz et al., as the authors also experience a similar ordering process, as Maschwitz observes for the thiourea additive, while both also evidence the additive to be located at the grain boundary. While I think that in-situ GIWAXS during to unravel the exact formation dynamics might be pretty challenging with an anti-solvent process, other strategies might be adapted to shed some light on the underlying mechanisms of the authors additive. Maybe the authors could employ in-situ solid-state NMR mixing experiments, or could calculate of the detachment energy and the ability of TDB (or TAB) to modify the ion transport across the grain boundaries. Is it possible to apply the additive on an already deposited layer? Maybe TDB could increase ion mobility supporting the halide mixture process, while TAB acts as an inhibitor delaying de-mixing?

Taken together, I believe that the findings of the authors can be suitable to be published in nature, if the manuscript is able to clarify the working mechanism of the additive both for reduced halides segregation and crystallization and further the authors can provide a certificate with proper measurement procedure (which would then also enter one of the well-known efficiency lists).

Referee #2

(Remarks to the Author)
This article demonstrates an interesting additive approach using the photo-transformable 4-[3-(trifluoromethyl)-3H-diazirin-3-yl]benzylamine hydrochloride (TDB) to retard halide segregation in wide-bandgap perovskites, achieving a certified 28.02% perovskite–organic tandem efficiency. The efficiency is quite remarkable; however, several critical concerns should be resolved before this article can be published in Nature.
1. (Originality)
The authors used 4-[3-(trifluoromethyl)-3H-diazirin-3-yl]benzylamine hydrochloride to suppress halide segregation and passivate point defects in perovskite materials. However, another group recently reported modulation of carrier dynamics and improvement of perovskite film quality and stability using 4-(3-(trifluoromethyl)-3H-diazirin-3-yl)benzylamine, which has exactly the same structure except for the presence of the HCl salt (Yang et al., Journal of Alloys and Compounds, 2025, 1048, 185243). Both molecules contain the same functional groups except for protonation, which means that the basic conceptual strategy for improving photovoltaic performance is quite similar. The authors should address this originality issue.
2. (Science)
Many photo-responsive and redox-active additives have been reported for stabilizing halide perovskites. For example, photochromic molecules in their open form (after illumination) have been shown to bond with perovskite materials and passivate point defects. In the case of TDB, what is the fundamental science that differs from previously reported photoactive passivation molecules? The authors need to clarify the special interaction between the functional groups and wide-bandgap halide perovskites from a scientific perspective (not only through simple bonding-energy simulations). Why is this TDB molecule particularly effective at suppressing halide-ion segregation? What is the rule of thumb?
3. (Evidence for the formation of TAB)
The authors indirectly demonstrated the formation of TAB in perovskite materials. While the formation of TAB as a molecule is acceptable, there is no direct evidence showing TAB formation within perovskite films during device operation. The authors should provide direct and quantitative evidence of TDB-to-TAB conversion in light-illuminated perovskite materials. Also, the authors mentioned that TAB is generated under UV illumination; however, in a solar simulator the UV portion is quite low. What fraction of TDB is converted under operando conditions?
4. (Provide the binding energy of TDB)
The authors compared the binding energies of TCB and TAB. For clarity, the binding energy of TDB should also be provided, and the interactions of all three molecules should be compared.
5. (Ambiguous explanation of halide segregation mechanism)
The authors state that TAB has a strong tendency to anchor at I vacancies, FA vacancies, and other defects, thereby pinning movable halide ions in the lattice. However, this explanation lacks scientific detail. Please explain this phenomenon more

clearly. What is the relationship between anchoring at FA vacancies and suppressing halide-ion migration?
6. (Effect of TAB on interfaces)
The TAB molecules may influence the interfaces between perovskite and the ETL or HTL. The authors should discuss the possible interactions between TAB and each transport layer.
7. (Stability of the tandem cell)
The authors provide stability data only under mild ISOS-L-1 conditions. For real applications, stability under harsher conditions (e.g., 85 °C/85% RH) is needed. Also, the MPPT duration of 300 s is not sufficient to demonstrate long-term stability.
8. (9 mm^2 cell size)
Many recent papers have reported module-scale or large-area devices. Although the >28% efficiency is high, the cell area is only ~9 mm^2. To demonstrate practical applicability, the authors are encouraged to present tandem-cell performance on a larger area.
9. (Typo)
- Misuse of “TBD” instead of TDB on page 14
- In Fig. 3i, please add a legend (“target” and “control”)
- “addictive” → additive on page 7

Version 1:

Reviewer comments:

Referee #1

(Remarks to the Author)
I commend the authors for a good job in unraveling the mechanisms at play in their devices. I recommend publication of the manuscript and look forward to its impact in the community.

Referee #2

(Remarks to the Author)
The authors have made a sincere effort to address the concerns raised by the reviewers, particularly by incorporating additional experimental results and expanding the discussion on the underlying mechanism. The distinction from previous studies is now more clearly presented, and the proposed two-stage mechanism based on the photo-transformable nature of TDB is supported by a variety of characterization techniques.
Nevertheless, the mechanistic understanding appears still somewhat descriptive in nature and may not yet reach a fully convincing or generalizable level. In particular, it remains somewhat unclear why this specific molecule exhibits a distinct advantage over previously reported photoactive additives, and a more clearly articulated design principle would be desirable. From this perspective, although the work is technically well executed, the level of fundamental insight may be somewhat limited.
Despite these points, the device performance is impressive and the overall body of supporting data is substantial. Therefore, the manuscript may be considered suitable for publication. However, minor revisions to further clarify the mechanistic framework and its broader implications would help to enhance the overall impact of the study.

Response to Reviewer #1:

I commend the authors for a good job in unraveling the mechanisms at play in their devices. I recommend publication of the manuscript and look forward to its impact in the community.

Response: We sincerely thank the reviewer for the positive comments and for recommending publication of our manuscript. We greatly appreciate the reviewer's careful assessment of our work and the constructive suggestions provided during the review process. These comments have been highly valuable in helping us improve our manuscript.

Response to Reviewer #2:

The authors have made a sincere effort to address the concerns raised by the reviewers, particularly by incorporating additional experimental results and expanding the discussion on the underlying mechanism. The distinction from previous studies is now more clearly presented, and the proposed two-stage mechanism based on the photo-transformable nature of TDB is supported by a variety of characterization techniques.
Nevertheless, the mechanistic understanding appears still somewhat descriptive in nature and may not yet reach a fully convincing or generalizable level. In particular, it remains somewhat unclear why this specific molecule exhibits a distinct advantage over previously reported photoactive additives, and a more clearly articulated design principle would be desirable. From this perspective, although the work is technically well executed, the level of fundamental insight may be somewhat limited.
Despite these points, the device performance is impressive and the overall body of supporting data is substantial. Therefore, the manuscript may be considered suitable for publication. However, minor revisions to further clarify the mechanistic framework and its broader implications would help to enhance the overall impact of the study.

Response: We sincerely thank the reviewer for this insightful and constructive comment. To address the reviewer's comment, we have further clarified the distinct advantages and design principle of TDB.

(1) Distinct advantage of TDB. The key feature of TDB is not merely its photoactivity, but its **stage-adaptive functionality**.

Previously reported photoactive additives mainly rely on photoisomerization {*Nat. Energy* 2026, 11, 623–632} (**Fig. R1a**), light-triggered defect passivation {*Adv. Mater.* 2022, 34, 2205338} (**Fig. R1b**) or photoinduced crosslinking {*Angew. Chem. Int. Ed.* 2025, 64, e202425578} (**Fig. R1c**) to modulate the as-formed perovskite film, thereby

improving the performance of single-junction perovskite solar cells.

In this work, with a focus on suppressing halide segregation in wide-bandgap (WBG) mixed-halide perovskites, TDB is designed to sequentially address **two different bottlenecks** in WBG mixed-halide perovskites: initial halide inhomogeneity during crystallization and defect-assisted halide segregation under operational illumination. Although these two stages are intrinsically separate, the photo-transformable nature of TDB bridges them by its **stage-adaptive functionality**.

During crystallization (Stage I), significant differences arise in the solubility and crystallization kinetics of PbI_2 and $PbBr_2$ precursors. The three-membered diazirine moiety of TDB engages in multisite interactions with lead halide and formamidinium iodide, suppressing the rapid precipitation of the Br-rich phase in the wet film and improving the initial halide homogeneity. During operation under illumination (Stage II), defects reduce the activation barrier for halide ion migration and thereby kinetically accelerate the halide segregation. Photo-transformable TDB accumulated at the grain boundaries is activated by the ultraviolet component of the solar spectrum and transforms into TAB. The resulting TAB, with a higher dipole moment, exhibits stronger adsorption on perovskite surfaces and increases the formation energy of iodide-related defects, thereby mitigating defect-assisted carrier trapping and halide-ion migration and suppressing the light-induced halide segregation in WBG perovskite.

Thus, TDB differs from previously reported photoactive additives by enabling stage-adaptive regulation across both film formation and device operation.

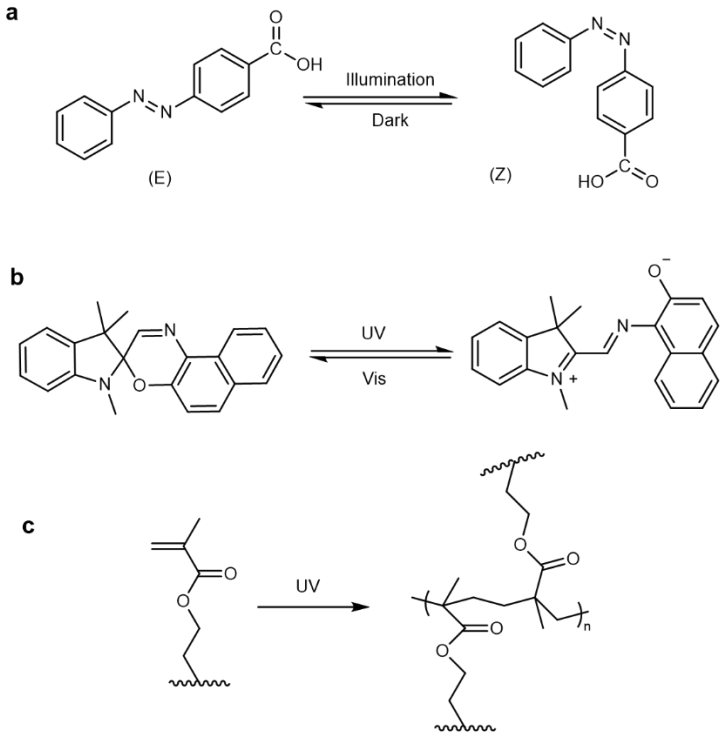

Fig. R1. Overview over structures of the photoactive agents reported in literature.

We have added the discussion in the revised manuscript on p.3: "Its photo-transformable nature enables stage-adaptive functionality, allowing TDB to sequentially address the challenges arising at two different stages in WBG mixed-halide perovskites."

(2) Design principle of TDB. The characteristic functionality of TDB mainly originates from the trifluoromethyl diazirine moiety, which is a well-established photoactive group.

The two electronegative N atoms of the trifluoromethyl diazirine moiety, which bear lone-pair electrons, can coordinate with Pb cations and act as dual hydrogen-bond acceptors for the N–H groups of FA^+, allowing TDB to interact with perovskite precursors during solution processing. These interactions allow TDB to regulate the crystallization process before photoconversion. Upon illumination, because of the photoactivity of trifluoromethyl diazirine moiety, TDB can undergo photo-transformation into TAB, a species with stronger adsorption on the perovskite surface.

Owing to its dual function, the trifluoromethyl diazirine moiety can serve as a potentially generalizable motif for designing photo-transformable additives, which can enable stage-adaptive regulation in WBG mixed-halide perovskites.

We have added the discussion in the revised manuscript on p.9: "Fortunately, beyond enabling interactions with perovskite precursors during solution processing, the trifluoromethyl diazirine moiety also serves as a well-established photoactive group. This key feature endows TDB with a photo-transformable nature, allowing TDB to transform into a new species under illumination containing ultraviolet components."

Response to reviewers:

Response to Reviewer #1:

In this manuscript present a new additive that improves efficiency and stability of wide gap perovskite solar cells and eventually enables impressive perovskite-organic tandem solar cells with an, to the best of my knowledge, unprecedented operation stability with a T_{90} of over 600h. As of that, I believe that this result is worth reporting and the nature family is a suitable platform for that, considering the enormous potential of perovskite-organic tandem solar cells – especially in the context of stability. Indeed extrapolated the authors stability seems to be almost at par with the current all-perovskite tandem record from Hairen's group (it should be expected to have something of 84% after 1000 h of stress). I would amend the authors to mention this aspect prominently, as it can motivate others to joint the community and contribute to its success.

Response: We appreciate the reviewer's thoughtful comments. We agree with the reviewer on the significance of the operational stability of perovskite–organic tandem solar cells (TSCs). As a new class of TSCs constructed from organic and organic–inorganic hybrid perovskite sub-cells, perovskite–organic TSCs hold great potential for operational stability. Motivated by these considerations, we performed the following additional investigations to provide more comprehensive evidence for the operational stability and intrinsic durability of the perovskite–organic TSCs.

(1). We fitted the degradation data using a biexponential empirical model, which has been widely adopted to describe non-linear performance decay in perovskite-based photovoltaic devices {*Science* 2022, *377*, 307–310}. Based on the fitted degradation trend under the ISOS-L-1 protocol, the perovskite–organic TSCs are projected to maintain over 85% of its initial performance after 1000 h of continuous MPP tracking under illumination (see **Fig. R1**). As the reviewer pointed out, our result is on par with the current record for all-perovskite TSCs from Hairen's group {*Nature* 2025, *648*, 600–606}.

We have also added the discussion in the revised manuscript on p. 15: "The TSCs maintained 90% of their initial efficiency after about 672 h of continuous illumination. By fitting the degradation data with a biexponential decay model ($R^2 > 0.95$), we extrapolated a projected T_{85} exceeding 1000 h (**Fig. 4g**), demonstrating strong stability under operational conditions."

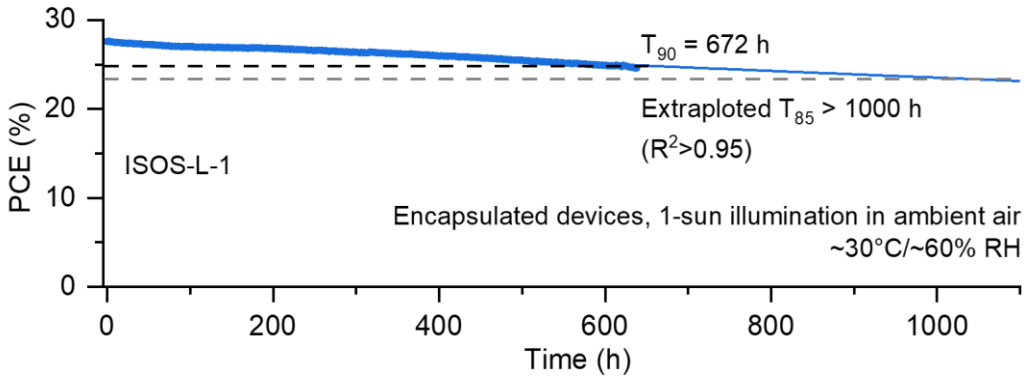

Figure. R1 (**Figure. 4g**). Long-term MPP tracking of the encapsulated perovskite–organic TSCs under simulated 1-sun illumination in ambient air without temperature control.

(2). We evaluated the thermal stability of encapsulated perovskite–organic TSCs under accelerated aging at 85 °C, following the ISOS-D-2 protocol. Under the thermal stress conditions, the encapsulated TSCs maintained over 80% of their initial performance after 600 h (T_{80} > 600 h), demonstrating the thermal robustness of the tandem architecture. (see **Fig. R2**)

We have added the discussion in the revised manuscript on p.16: "Under accelerated aging at 85 °C (ISOS-D-2), the encapsulated TSCs maintained over 80% of their initial performance after 600 h, demonstrating the thermal robustness of the tandem architecture (**Fig. 4h**)."

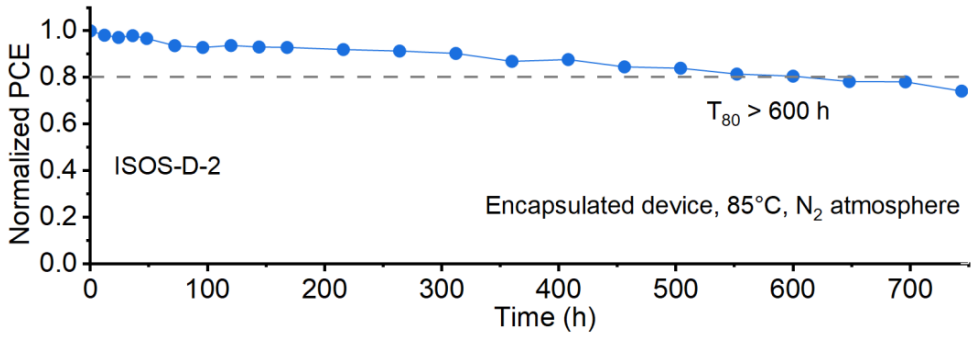

Figure R2 (**Figure. 4h**). Operational stability of encapsulated perovskite–organic TSCs under accelerated aging at 85 °C, following the ISOS-D-2 protocol.

(3). We supplemented the manuscript with experiments supporting the intrinsic stability potential of perovskite–organic TSCs, especially the complementary properties of the WBG perovskite front cell and NBG organic rear cell.

Firstly, the WBG perovskite front cell can filter ultraviolet light and a fraction of the visible spectrum, thereby shielding the NBG organic rear cell from high-energy-photon-induced

degradation, which is among the most detrimental stress factors for OSCs. {*J. Mater. Chem. A* 2021, *9*, 19778–19787}, {*Nature* 2022, *604*, 280–286}. We placed quartz substrates coated with WBG perovskite films (encapsulated) in front of encapsulated OSCs in ambient air, simulating the spectral filtering scenario in the TSCs. Under continuous MPP tracking, the filtered organic device maintained over 95% of its initial output power for over 1100 h (T_{95} > 1100 h). In contrast, the OSCs without WBG perovskite filtering degraded to 84% of its initial efficiency after 550 h (see **Fig. R3**).

We have added the Supplementary Fig. 41 in SI.

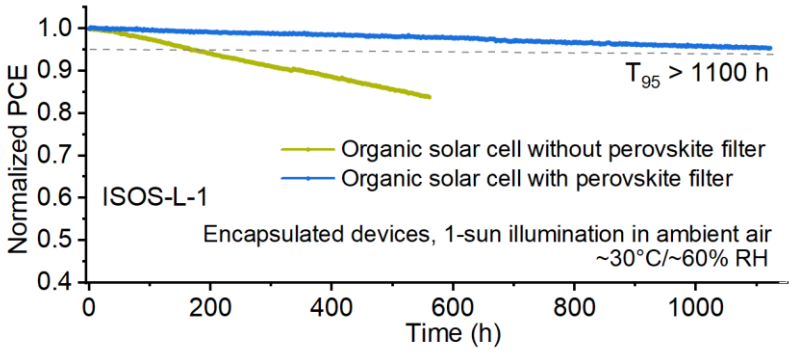

Figure R3 (**Supplementary Figure. 41**). Long-term MPP tracking of the encapsulated OSC without and with a WBG perovskite filter under simulated 1-sun illumination in ambient air.

Secondly, we investigated the operational stability advantage of perovskite–organic TSCs under high-humidity conditions due to the hydrophobic properties of the organic rear cell. The ~120 nm-thick organic active layer acts as an additional barrier shielding the perovskite front cell from moisture—a detrimental stress factor that can trigger perovskite decomposition {*Sci. Adv.* 2025, *11*, eady5703}. We conducted accelerated aging tests under 85% relative humidity (RH) in ambient air. When comparing unencapsulated WBG perovskite single-junction devices with unencapsulated perovskite–organic TSCs, the WBG perovskite single-junction devices exhibited a rapid performance decline within the first 12 h. In contrast, the unencapsulated perovskite–organic TSCs showed markedly improved storage stability under the same high-humidity conditions (see **Fig. R4**).

We have added the Supplementary Fig. 42 in SI.

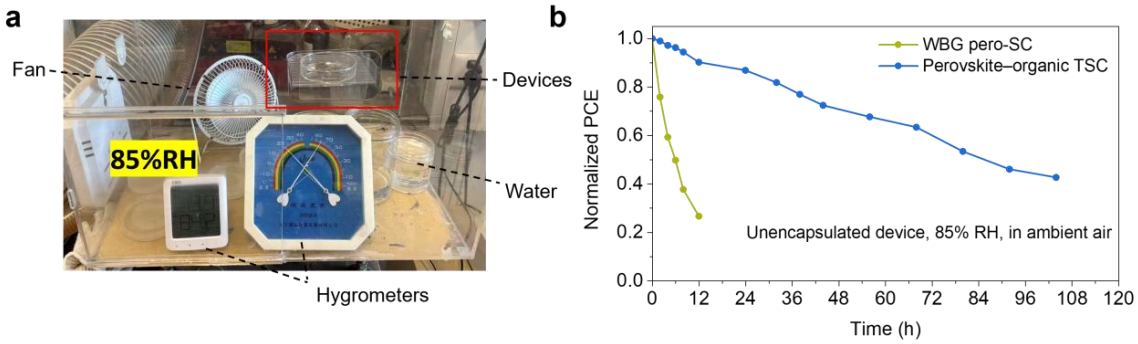

Figure R4. (**Supplementary Figure. 42**) **a,** Photograph of the humidity-controlled setup. There are devices, water, hygrometers and fan in the storage box. **b**, Operational stability of unencapsulated WBG perovskite-SCs and unencapsulated perovskite–organic TSCs under high-humidity accelerated aging condition.

Within only 12 h, the perovskite absorber visibly transformed from the black perovskite phase to yellow PbI_2 under the high-humidity conditions, concurrently, the Ag electrode exhibited obvious degradation. In contrast, the perovskite absorber in the unencapsulated perovskite–organic TSCs retained its black phase under the same high-humidity conditions (see **Fig. R5**).

We have added the Supplementary Fig. 43 in SI.

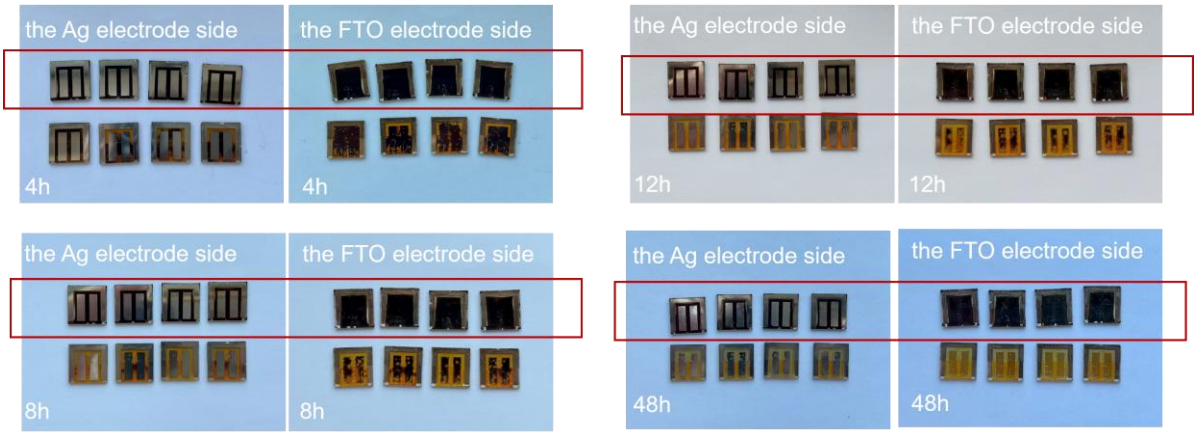

Figure R5 (**Supplementary Figure. 43**). Photograph of devices under high-humidity accelerated aging condition (85% RH in ambient air). The perovskite–organic TSCs are enclosed in the red box in the photograph, with the WBG perovskite-SCs located below.

Another very important aspect is the choice of solar cell calibration. Curiously for some reason, currently the community is moving backwards with respect to reliability especially of multi-junction solar cell data. The Calibration certificate that the authors provide does not contain a measurement of the quantum efficiency, which casts doubt, that the calibration has been performed under properly adjusted light sources (see e.g. 10.1002/solr.202200800). Not following proper measurement protocols, has unfortunately led to a situation, where the progress of the field is currently not reflected in well-accepted collections as the NREL efficiency chart or the Green solar cell efficiency tables. On top of that, the authors are actually stating the reverse scan of the calibration, instead of the stabilized value (which is 27.6%, if I calculated correctly from the certificate). If the main reason for publication of a study is the efficiency, every author has to take extra care, that it is measured correctly. I can only recommend publication on this motivation, if a well accepted calibration protocol is used.

Response: We sincerely thank the reviewer for this comment regarding calibration protocols and data reliability for multi-junction solar cells. In response, we submitted representative devices for independent certification at the National Photovoltaic Industry Measurement and Test Center (NPVM), which is one of the nine internationally recognized laboratories acknowledged by the Solar Cell Efficiency Tables ("Martin Green Table").

The **certified steady-state efficiency** of our representative perovskite–organic TSC reached **28.04%**, and this certificate includes **quantum efficiency measurements** for the measured sample, which is used to calculate the spectral mismatch factor and thus correct the simulator's nonideal spectral irradiance distribution. We believe this third-party certification further substantiates the performance reported in our study and will also help researchers in the community to recognize the standardized certification protocols for multi-junction solar cells (see **Fig. R6**).

We agree that the steady-state certified value should be emphasized rather than the reverse-scan value, and we have revised the manuscript accordingly on p.15: "The device efficiency was further certified at National Photovoltaic Industry Measurement Test Center (NPVM) with a steady-state PCE of 28.04% (Supplementary Fig. 44)", we have also updated the data in **Fig. 4d** and Supplementary Table 8 and we have added Supplementary Fig. 44 in SI.

Figure R6 (**Supplementary Figure. 44**). The certificate of our representative perovskite–organic TSC with steady-state PCE of 28.04% from the National Photovoltaic Industry Measurement and Test Center (NPVM). The certificate also includes the measurement of relative spectral responsivity for the measured device, which is used to calculate the spectral mismatch factor and thus correct the simulator's nonideal spectral irradiance distribution.

That's also where the trouble begins - while the devices are nature level, the science behind these devices still needs some serious work-over and additional insights – Afterall a scientific paper should not only state a result, but also unravel the underlying mechanisms. From a birds-view perspective, the authors mainly elaborate on the effect of their TDB additive – anyhow towards the mechanism that is actually at play here remains elusive and the discussion remains rather superficial and contains a lot of speculation, that is sometimes in contradictions to recent findings in the field.

Two key topics and key issues here are the crystallization mechanism and the halide segregation topic, that I will address separately here:

Halide segregation:

Here the authors consistently reproduce a common misconception on the origin and damage mechanism of halide segregation, that has been miss-proven for quite a while now. As shown e.g. 10.1021/acsenergylett.0c01104, recombination is actually not the key issue in a halide segregated solar cell – the authors unfortunately only show the development of the PCE data and only fast hysteresis of fresh devices (leaving out J_{sc}, which I don't understand), but in my experience halide segregation typically strongly impacts on J_{sc}, as it increases the amount of mobile ions and increases ionic losses (see 10.1038/s41560-024-01487-w).
In general the discussion on the topic is relatively thin, taking into account that there has been extensive studies and reviews on halides segregations (one even targeting perovskite-organic tandems e.g. in 10.1038/s41578-023-00642-1) and by the use of e.g. redox shuttles to reintegrate oxidized species (10.1038/s41560-024-01451-8) there have already been targeted strategies to overcome the root cause of halide segregation. The observed photoactivity of the TDB molecule appears to be interesting, but the mere fact that it sits at the grain boundary is not a mechanism and does not explain, how it is able to reduce the oxidization of iodide or the formation of hole accumulations. The authors should provide an in-depth study on how this molecule can tackle the root cause of halide segregation, taking into account up to date literature on the topic and building from it.

Response: We sincerely thank the reviewer for this insightful and constructive comment on halide segregation. Our response is organized around **two points**.

First, we agree that recombination is not the dominant manifestation of halide segregation in operating devices, we provide device-level evidence showing that the detrimental impact of halide segregation is more directly reflected in **enhanced ion migration and ionic losses**, rather than in recombination loss alone.

Second, we clarify **a two-stage mechanistic picture arising from the photo-transformable nature of TDB**, in which TDB improves the initial halide mixing during crystallization, while the photo-converted TAB suppresses defect-assisted halide de-mixing under illumination.

In the following, we discuss these two points in turn.

(1). We extracted the relative loss trends of V_{oc}, J_{sc}, and FF during MPP tracking testing for the control and target WBG pero-SCs (see **Fig. R7**). In both devices, the decrease in J_{sc} was the most pronounced among the three parameters. This result indicates that ion-induced electric-field screening, driven by ion migration under illumination, makes the largest contribution to the overall performance degradation {*Nat. Energy* 2024, *9*, 595–605}.

We have added the Supplementary Fig. 34 in SI.

We have added the discussion in the revised manuscript in p.3: "Meanwhile, defects reduce the activation barrier for halide ion migration[18] and thereby kinetically accelerating the halide segregation[19] which in turn induces more halide defects and mobile ions. Under operational conditions, these mobile ions lead to ion-induced electric-field screening, thereby reducing charge-collection efficiency and accelerates device degradation[20]."

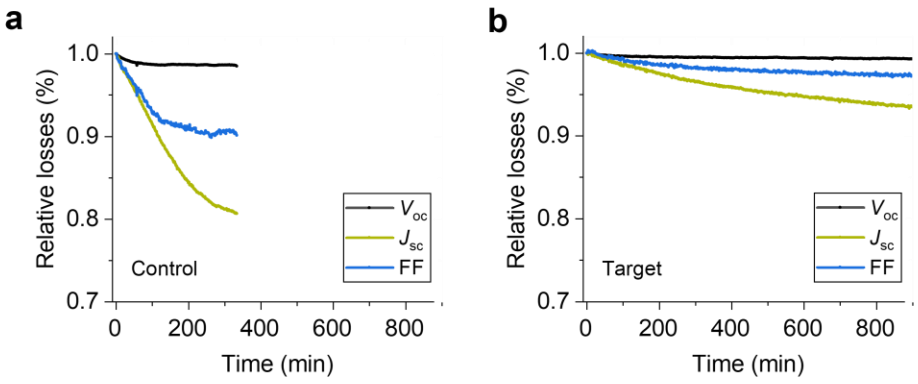

Figure R7 (Supplementary Figure. 34). The relative loss trends of V_{oc}, J_{sc}, and FF during MPP tracking testing for the control and target WBG pero-SCs.

We also completed the manuscript by adding the scan-rate-dependent J_{sc}, V_{oc}, FF and PCE of the **fresh and aged** WBG pero-SCs for the control and target devices (see **Figs. R8 and R9**). Notably, the control devices showed a pronounced J_{sc} loss at low scan rates even before light-soaking aging, indicating substantial ionic effects likely arising from the initially inhomogeneous halide distribution. After aging, this scan-rate dependence became much stronger, suggesting more severe phase segregation and greater ionic losses in the control devices. In contrast, the target devices showed much weaker scan-rate dependence in both the fresh and aged states,

consistent with improved initial halide homogeneity and reduced light-induced halide de-mixing.

We have added Supplementary Figs. 35 and 36 in SI.

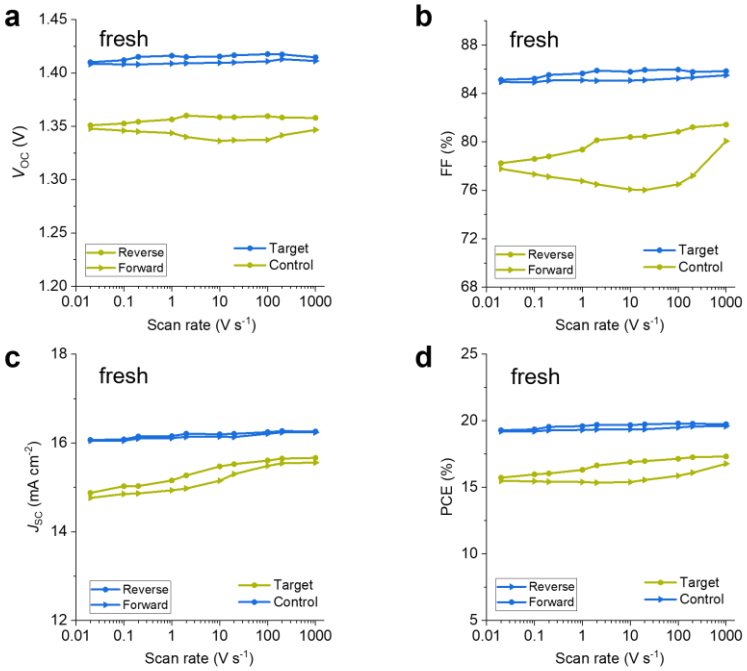

Figure R8 (Supplementary Figure. 35). V_{oc}, FF, J_{sc} and PCE of fresh control and target WBG pero-SCs (before aging under 1-sun MPP tracking), measured at a scan rate ranging from about 0.01 V s^{-1} to 1,000 V s^{-1} in reverse and forward sweep directions.

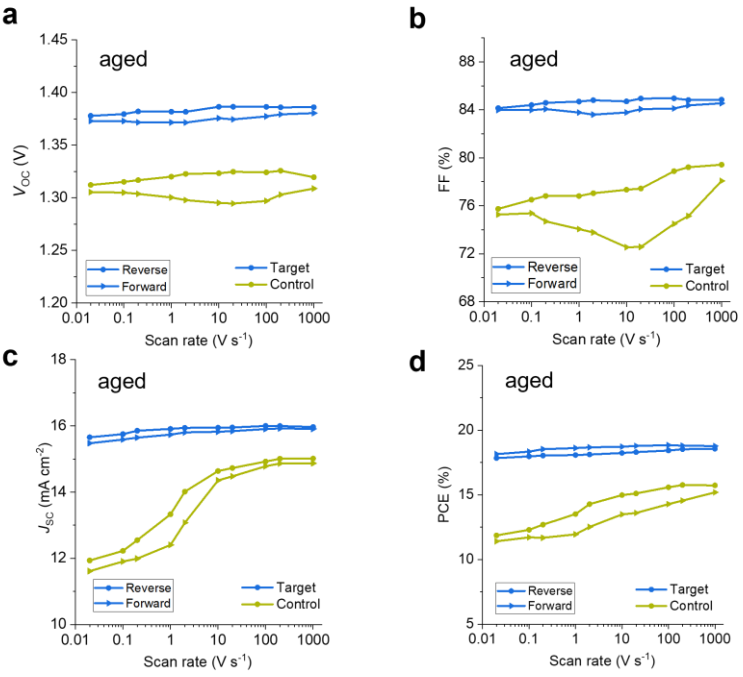

Figure R9 (Supplementary Figure. 36). V_{oc}, FF, J_{sc} and PCE of aged control and target WBG

pero-SCs (after 12 h of aging under 1-sun MPP tracking), measured at a scan rate ranging from about 0.01 V s^{-1} to 1,000 V s^{-1} in reverse and forward sweep directions.

(2). We propose a two-stage strategy enabled by the photo-transformable property of TDB to suppress halide segregation in high-Br-content WBG perovskites.

First, during the crystallization stage, TDB **promoting more homogeneous halide mixing** in the as-formed perovskite film. This view is supported by multiple lines of evidence, including *in situ* GIWAXS, solid-state ^{207}Pb NMR and DFT calculations, as discussed in detail below in our response to the comment on the crystallization mechanism.

Second, during operation under illumination, TDB undergoes photo-conversion to form TAB. TAB possesses a larger dipole moment and stronger adsorption on the perovskite surface than TDB, and therefore no longer acts as a dynamic mediator for halide mixing. Instead, owing to its stronger anchoring at surface defect sites, TAB increases the formation energies of iodine vacancies and iodine interstitials, which are key defects involved in halide migration, thereby **suppressing defect-assisted halide de-mixing**.

We have added the discussion in the revised manuscript in p.2: "Here, we introduced a photo-transformable additive 4-[3-(trifluoromethyl)-3H-diazirin-3-yl]benzylamine (TDB) into the WBG perovskite precursor solution to establish a two-stage strategy for stabilizing the mixed-halide phase. During crystallization, TDB initial halide homogeneity by suppressing the rapid precipitation of the Br-rich phase in the wet film and accelerating halide mixing during annealing; during operation under illumination, TDB undergoes transformation to form a new species with stronger adsorption on the perovskite surface, which inhibits the formation of iodide related defects, suppresses defect-assisted carrier trapping and ion migration and thereby mitigates light-induced halide segregation[9,10]."

We have added the discussion in the revised manuscript in p.3: "Here we introduced 4-[3-(trifluoromethyl)-3H-diazirin-3-yl]benzylamine (TDB), an aromatic ammonium cation with deliberately designed functional groups, into the WBG perovskite precursor solution. During crystallization, TDB features a three-membered diazirine engages in multisite interactions with FAI and lead halides, thereby suppressing the rapid precipitation of the Br-rich phase in the wet film. This wet-film state with homogeneous phase distribution provides a foundation for halide mixing during annealing, thereby improving the halide homogeneity of the final film."

We have also added the discussion in the revised manuscript in p.4: "The newly generated TAB with higher dipole moment exhibits stronger adsorption on the perovskite surface and increases the formation energy of iodine-related defects, thereby suppressing defect-assisted carrier trapped and halide-ion migration, consequently enhances the photo-stability of the WBG perovskite."

We discuss the second stage under operation under illumination in detail below.

Owing to the photo-transformable nature of TDB, reactions occur under illumination and generate new species, we called this TAB. The electron-withdrawing carbonyl group in TAB increases the maximum electrostatic potential on the ammonium side while lowering the minimum electrostatic potential on the opposite side, thereby giving TAB a larger dipole moment than TDB (see **Fig. R10a,b,** and **Table R1**). This enlarged dipole strengthens the electrostatic interaction between the ammonium group and the perovskite surface. In addition, the carbonyl oxygen can further coordinate with undercoordinated Pb sites, giving rise to a multisite anchor mode. DFT calculations reveal that TAB exhibits a shorter binding distance and stronger adsorption on the perovskite surface than TDB (see **Fig. R10c,d,** and **Table R1**). More importantly, TAB treatment increases the formation energies of iodine vacancies and iodine interstitials (see **Fig. R11**). The suppression of these iodide-related defects mitigates defect-assisted carrier trapped, which is expected to reduce the free-energy gain of the de-mixing state. Meanwhile, the reduced defect density also inhibits defect-mediated halide-ion migration, thereby suppressing phase segregation under illumination.

We have added Supplementary Fig. 30.

We have added Supplementary Table. 4

We have added the discussion in the revised manuscript in p.12: "DFT calculations indicate that TAB possesses a larger dipole moment (**Fig. 3b**) and stronger adsorption on the perovskite surface than TDB (**Fig. 3c,d** and data is shown in Supplementary Table. 4), owing to its multisite anchoring mode involving electrostatic interaction through the ammonium group together with additional coordination of the carbonyl oxygen to undercoordinated Pb sites. X-ray photoelectron spectroscopy (XPS) measurements also demonstrated these results (Supplementary Fig. 29). Moreover, TAB increases the formation energies of iodine vacancies and iodine interstitials (Supplementary Fig. 30)."

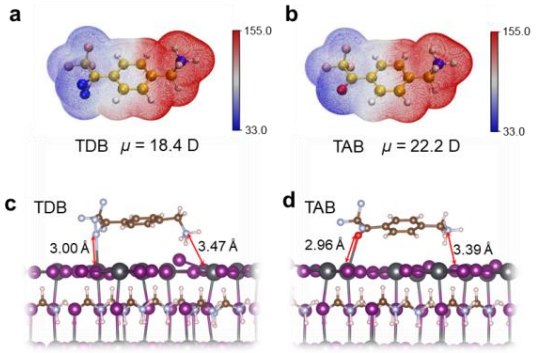

Figure R10 (**Figure 3b-d**). Electrostatic potential surfaces of (**a**) TDB and (**b**) TAB. Calculated adsorption models of (**c**) TDB and (**d**) TAB on the perovskite surface.

Table R1 (**Supplementary Table. 4**). the maximum and minimum points (φ_{max} and φ_{min}) of the electrostatic potential and adsorption energy of TAB and TDB.

molecule	φ_{max} (kcal/mol)	φ_{min}(kcal/mol)	adsorption energies
TAB	158.1	31.1	-8.2 eV
TDB	154.8	33.4	-6.9 eV

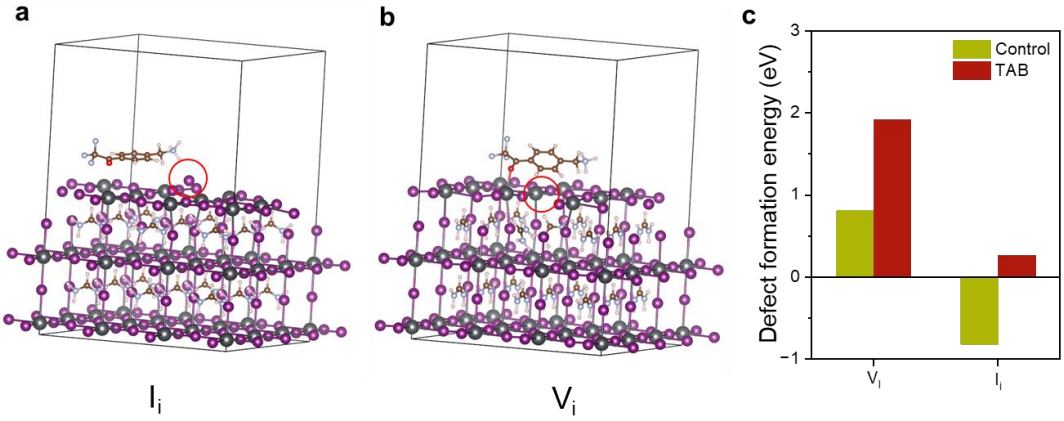

Figure R11 (**Supplementary Figure. 30**). **a,b,** Optimized structures of TAB adsorbed on the perovskite surface with iodide interstitial and iodide vacancy, respectively. **c,** Calculated formation energies of V_I and I_i of the control and TAB-treated perovskites.

We performed Transient photocurrent (TPC) measurements (see **Fig. R12**) to confirm the inhibited defect-assisted carrier trapping. The shortest decay time observed for the TAB-treated device suggests reduced defect-assisted carrier trapping and charge accumulation.

We have added the discussion in the revised manuscript in p.12: "The suppression of these iodide-related defects mitigates defect-assisted carrier trapping. Transient photocurrent (TPC) measurements (Supplementary Figure. 31) were performed on the control, TDB-treated, and TAB-treated pero-SCs. The shortest decay time observed for the TAB-treated device suggests reduced defect-assisted carrier trapping and charge accumulation[36]. Meanwhile, the reduced defect density also suppresses defect-mediated halide-ion migration[37]."

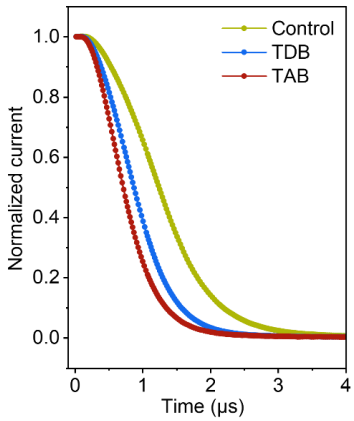

Figure R12 (**Supplementary Figure 31**). Transient photocurrent (TPC) measurements for the control, TDB-treated, and TAB-treated pero-SC devices. The normalized TPC decay curves were fitted with a single-exponential function, yielding characteristic decay times of approximately 1.10, 0.86, and 0.68 μs, respectively.

We performed continuous-illumination PL measurements to directly confirm that TAB suppresses light-induced phase segregation effectively (see **Fig. R13**). We prepared control, TAB-treated, and TDB-treated perovskite films, in which TAB or TDB was spin-coated from IPA solution onto pristine perovskite films as a surface treatment. Under continuous 1-sun illumination, the control film developed an additional emission peak at ~740 nm, assigned to an I-rich phase, which dominated the spectrum after 20 min. In contrast, the TAB-treated film showed a much lower extent of halide segregation, with almost no red-shifted peak observed throughout the measurement. Although TDB treatment also showed a certain ability to suppress phase segregation, its effect was clearly less pronounced than that of TAB. This trend is further supported by the evolution of the I-rich-to-intrinsic peak ratio and is consistent with the above theoretical analysis.

We have added the discussion in the revised manuscript in p.13: "Continuous-illumination PL measurements were performed to directly verify the role of TAB in suppressing phase segregation (**Fig. 3e-g**). While the control film developed a pronounced red-shifted emission at ~740 nm, assigned to an I-rich phase, the TAB-treated film showed almost no such peak throughout the measurement. Although TDB treatment also showed a certain ability to suppress phase segregation, its effect was clearly less pronounced than that of TAB. This trend is further supported by the evolution of the I-rich-to-intrinsic peak ratio (Supplementary Fig. 33) and is consistent with the above theoretical analysis."

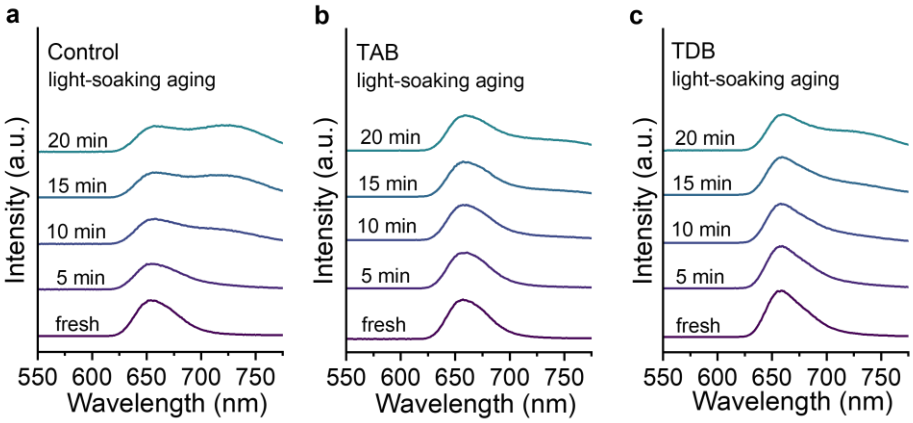

Figure R13 (**Figures. 3e-g**). PL evolution for control, TAB and TDB treated perovskite films after light soaking under 1-sun illumination for 20 minutes.

Furthermore, we compared the scan-rate-dependent J_{sc} of devices measured before and after aging (see **Fig. R14**). Even in the fresh state, the target devices already showed weaker scan-rate dependence than the control devices, indicating reduced ionic losses in the initially formed devices, which is consistent with the role of TDB in promoting more homogeneous halide mixing during film formation. After 24 h of aging, this contrast became even more pronounced, with the control devices exhibiting much stronger scan-rate dependence, indicating more severe ion-related losses that are consistent with increasing phase segregation during operation. This device-level behavior further supports the synergistic roles of TDB in improving the initial halide homogeneity and TAB in suppressing defect-assisted halide de-mixing under illumination.

We have added the discussion in the revised manuscript in p.13: "Furthermore, we compared the scan-rate-dependent J_{sc} of devices measured before and after aging (**Figs. 3h,i**). Even in the fresh state, the target devices already showed weaker scan-rate dependence than the control devices, indicating reduced ionic losses in the initially formed devices, which is consistent with the role of TDB in promoting more homogeneous halide mixing during film formation. After 12 h of aging, this contrast became even more pronounced, with the control devices exhibiting much stronger scan-rate dependence, indicating more severe ion-related losses that are consistent with increasing phase segregation during operation[20]. This behavior further supports the synergistic roles of TDB in improving the initial halide homogeneity and TAB in suppressing defect-assisted halide de-mixing under illumination."

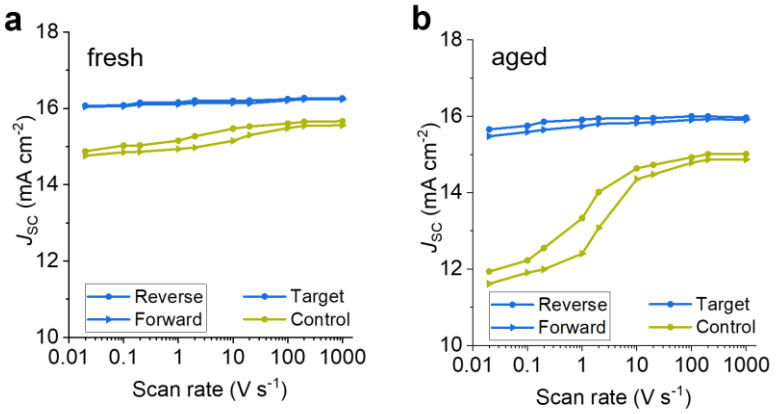

Figure R14 (**Figures. 3h,i**) Comparison of the scan-rate-dependent J_{sc} of control and target WBG pero-SCs before (**a**) and after aging (**b**).

To assess the phase separation in the WBG front-cell after aging in the integrated tandem architecture, we measured the electroluminescence (EL) characteristics of the control and target perovskite–organic TSCs after aging under ISOS-L-1 protocol (see **Fig. R14)** The aged control device exhibited an additional emission peak at ~740 nm, assigned to an I-rich phase, across different injection current densities, indicating pronounced phase segregation after light-soaking aging. By contrast, the EL peak of the WBG front cell in the target device retained its position with increasing injection current density. These results indicate that the target device remains more resistant to bias-induced phase segregation even after light-soaking aging.

We have added the discussion in the revised manuscript on p.15: "We measured the EL spectra of the control and target perovskite–organic TSCs after 240 h of ISOS-L-1 aging to probe phase segregation of the WBG front cell in aged integrated tandem devices (**Fig. 4e,f**). The aged control device exhibited an additional emission peak at ~740 nm across different injection current densities, which is assigned to an I-rich phase. However, the target device retained a stable EL peak position indicating that the target device remains more resistant to bias-induced phase segregation even after light-soaking aging[42]."

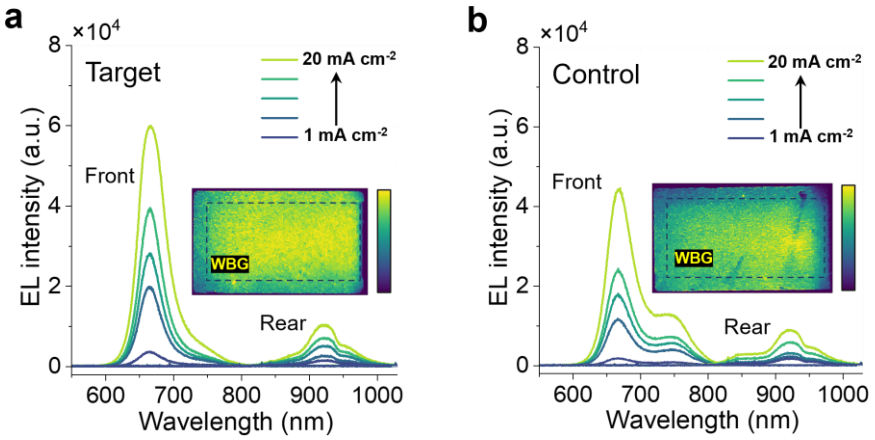

Figure. R15 (**Figure. 4e,f**). EL spectra of the aged (**a**) control and (**b**) target perovskite–organic TSCs measured at different injection current densities for the front and rear sub-cells. Inset: EL image of the WBG perovskite front cell.

Crystallization:

Here the manuscript similarly shows an incomplete discussion and in part bases their hypothesis on incomplete and outdated hypothesis. One of the key points of argumentation that the authors use to argument the beneficial effect of their TDB molecule is an interaction inside the solution. Now there has been a very recent study demonstrating, that such deductions are not valid, as firstly the interaction in the perovskite precursor solution are highly complex due to the formation of solvates (see e.g. 10.1021/acs.jpclett.0c03741, which the authors don't account for) and, most importantly, secondly largely unrelated to the final crystal formation process (10.1038/s41467-025-65484-7). Actually in-situ GIWAXS studies on mixed halide perovskites (10.1021/acsami.3c18623) straightforward show, that a segregated initial stage is pretty common when depositing wide gap perovskites and the formation of the final mixed perovskite occurs during annealing. Throughout the manuscript the authors argument with "nucleation" of the perovskite and "preferred formation of Br-rich nuclei" etc. without having any way of measuring the process of nucleation, which occurs at the very moment of anti-solvent exposure. A transition from the delta to the alpha phase is certainly not a nucleation process. Also the process of halide mixing during annealing cannot be explained by nucleation. Rather it is a reorganization of the already existing crystal structure, which would most probably involve additive driven grain coarsening (see 10.1038/s41467-025-65484-7). Indeed there is some striking resemblance between this work and the work from Maschwitz et al., as the authors also experience a similar ordering process, as Maschwitz observes for the thiourea additive, while both also evidence the additive to be located at the grain boundary. While I think that in-situ GIWAXS during to unravel the exact formation dynamics might be pretty challenging with an anti-solvent process, other strategies might be adapted to shed some light on the underlying mechanisms of the authors additive. Maybe the authors could employ in-situ solid-state NMR mixing experiments, or could calculate of the detachment energy and the ability of TDB (or TAB) to modify the ion transport across the grain boundaries. Is it possible to apply the additive on an already deposited layer? Maybe TDB could increase ion mobility supporting the halide mixture process, while TAB acts as an inhibitor delaying de-mixing?

Response: We sincerely thank the reviewer for this insightful suggestion. We agree that the beneficial role of TDB should not be primarily interpreted in terms of simple precursor-solution interactions or unresolved nucleation arguments. Instead, guided by the reviewer's suggestion and our further analysis, we have revised this part of the manuscript to focus on **halide mixing during annealing**. Full-process *in situ* GIWAXS directly tracks the phase evolution and halide-mixing behavior during spin-coating and annealing, while ^{207}Pb solid-state NMR reveals the evolution of the local Pb–halide coordination environment toward a mixed-halide state. These results indicate

that the mixed-halide phase in high-Br WBG perovskites is mainly established during annealing, and that TDB accelerates this process, thereby improving the initial phase homogeneity of the as-formed film. Combined with the discussion above on the role of TAB, discussion in this part below will further supports our proposed two-stage strategy, in which TDB facilitates halide mixing during annealing, whereas the photo-converted TAB suppresses halide de-mixing under illumination.

(1). To clarify the phase evolution process, we performed synchrotron-based *in situ* GIWAXS measurements to monitor the annealing behavior of high-Br WBG perovskites in real time. With increasing Br content in the $FAPb(I_{1-x}Br_x)_3$ system (20 mol% MACl was introduced to assist crystallization), the crystallization pathway changed. For $FAPbI_3$, the wet film after antisolvent quenching exhibited the δ phase, which gradually transformed into the α phase during annealing. Higher-Br films crystallized much more rapidly and directly formed the α phase without a detectable δ-phase intermediate (see **Fig. R16**). Notably, the 50 mol% Br WBG perovskites already exhibited severe phase separation in the wet-film state before annealing and still showed clear phase separation after annealing, indicating its strong intrinsic tendency toward halide segregation. This observation prompted us to further investigate this process.

We have added Supplementary Fig. 1 in SI.

We have added the discussion in the revised manuscript on p.4: "To investigate how the crystallization process influences phase separation in WBG perovskite with 50 mol% Br, we carried out *in situ* grazing incidence wide-angle X-ray scattering (GIWAXS) measurements. Pronounced phase separation was observed already in the wet-film state after spin-coating and persisted after annealing (Supplementary Fig. 1). Based on these results, we focused on the (i) spin-coating and (ii) annealing processes to track the phase evolution. The untreated precursor solution ($FA_{0.8}Cs_{0.2}Rb_{0.1}Pb(I_{0.5}Br_{0.5})_3$) was used as the control for crystallization observation."

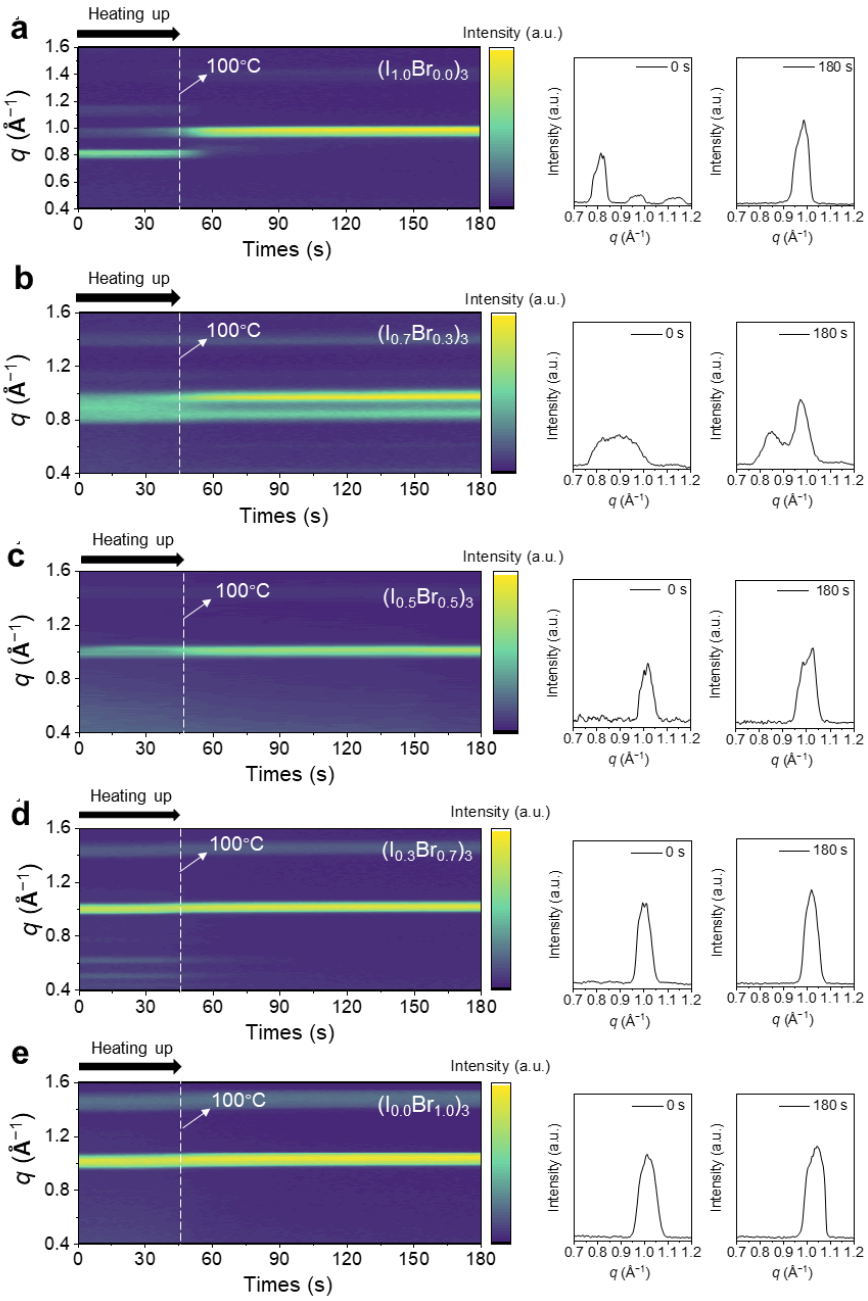

Figure R16 (**Supplementary Figure. 1**). *In situ* GIWAXS patterns recorded during the annealing process of WBG perovskite films with different I/Br ratios (20 mol% MACl was introduced to assist crystallization). Heating was started at 0 s from room temperature. The dashed line marks the time point (40 s) when the temperature reached 100 °C, followed by annealing at 100 °C for 140 s.

(2). We devoted efforts to design an *in situ* GIWAXS sample chamber equipped with a spin coater and an antisolvent syringe under a N_2 atmosphere, allowing recording the **full process from spin-coating to annealing.**

As shown in **Fig. R17**, the wet films exhibited a single diffraction peak immediately after antisolvent dripping. However, once spinning stopped, this initially single peak immediately split into two distinct peaks corresponding to Br-rich and I-rich phases (see **Fig. R17b**), indicating that the reducedn solvent evaporation rate after spinning amplified the solubility disparity between the two phases. A similar phenomenon was also observed in the *in situ* PL measurements during spin-coating (see **Fig. R18**). During annealing, the diffraction peak of the control sample broadened at the early stage, indicating the onset of halide mixing together with local variations in unit-cell size{*Energy Environ. Sci.* 2025, *18*, 10460–10472}. With prolonged annealing, the peak gradually narrowed and shifted toward lower q values, reflecting the gradual incorporation of iodide into the perovskite lattice. Nevertheless, the control sample exhibited slow mixing kinetics and did not evolve into a homogeneous mixed-halide phase within the annealing time (see **Fig. R17c,d**).

To improve the initial halide homogeneity of the WBG perovskite, we introduced TDB into the precursor solution. Although some peak broadening was also observed in the TDB-treated wet film after spinning, the diffraction feature could still be mainly assigned to a mixed-halide phase, with only minor variation (see **Fig. R17e,f**). During annealing, the TDB-treated film showed much faster halide-mixing kinetics than the control and ultimately evolved into a single diffraction peak, indicative of a more homogeneous mixed-halide phase (see **Fig. R17g,h**).

We have added Supplementary Fig. 2 in SI.

We have added the discussion in the revised manuscript on p.4: "Firstly, during spin-coating (**Fig. 1a**), the wet films of control sample exhibited a single diffraction peak after antisolvent dripping without detectable δ phase or solvent-associated intermediate phase. Once spinning stopped, this single peak immediately split into two distinct peaks (**Fig. 1b**), indicating clear phase separation. A similar transition was also observed in the *in situ* PL measurements (Supplementary Fig. 2). We infer that the slower solvent evaporation after spinning amplified the solubility disparity between the Br-rich and I-rich phases, while the faster crystallization of the Br-rich phase further promoted its precipitation. Secondly, during annealing (**Fig. 1c**), the phase separation inherited from the wet-film persisted. Then, the diffraction peak of the film broadened, which indicated the onset of halide mixing[21] and gradually narrowed with prolonged annealing. Nevertheless, the diffraction peak of the control sample remained noticeably broadened (**Fig. 1d**) rather than evolving into a sharp single peak characteristic, indicating incomplete halide homogenization."

We have added the discussion in the revised manuscript on p.5: "To investigate how TDB influenced the crystallization of high-Br-content WBG perovskite, we introduced TDB into the precursor solution and monitored the crystallization process by *in situ* GIWAXS. Firstly, the spin-coating process was shown in **Fig. 1e**, although some peak broadening was observed in the TDB-treated wet film after spinning, the diffraction feature could still be mainly assigned to a mixed-halide phase, with only minor variation (**Fig. 1f**), indicating the TDB-treated wet film retains a

stabilized mixed-halide phase without obvious segregation, which arise from the interactions of TDB with FA and lead halides, enabled by the two electron-rich N atoms in the diazirine unit. These interactions help suppress the rapid precipitation of the Br-rich phase, thereby stabilizing the mixed-halide phase during spin-coating process. This wet-film state with homogeneous phase distribution provides a foundation for halide mixing during annealing, thereby contributing to the improved halide homogeneity of the final film."

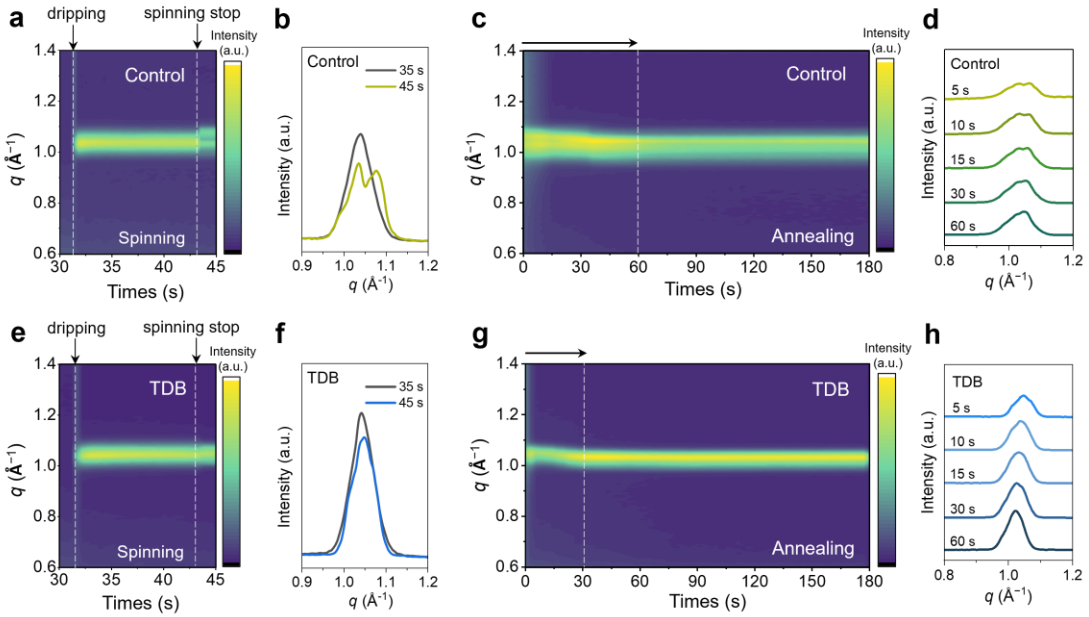

Figure R17 (Figure 1a-h). *In situ* GIWAXS patterns recorded during the spin-coating of wet perovskite films ($FA_{0.8}Cs_{0.2}Pb(I_{0.5}Br_{0.5})_3$) without and with TDB treatment. Antisolvent dripped at 31 s; spin-coating stopped at 43 s.

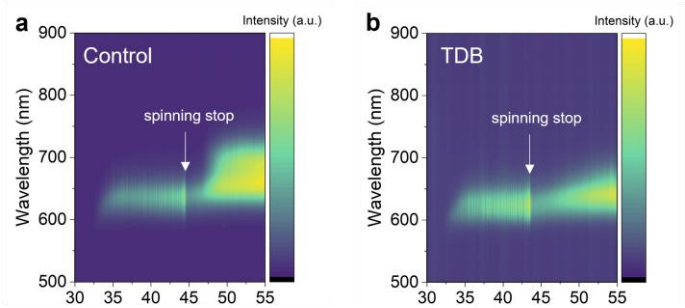

Figure R18 (Supplementary Figure 2) *In situ* PL characterization of phase evolution in control and TDB-treated WBG perovskite films during spin-coating.

(3). The TDB-treated 50 mol% Br WBG perovskites exhibited less pronounced phase separation both in the wet-film state and the final film. The weaker phase separation in the TDB-treated wet film may arise from the interaction between TDB and FA^+, which could retard crystallization{s41560-026-02010-z} and narrow the kinetic disparity between the precipitation

of the Br-rich and I-rich phases (Supplementary Fig. 3), but this effect is unlikely to be the dominant origin of the improved final halide mixing. Instead, the halide mixing during annealing is more likely governed by a reorganization of the pre-existing crystal structure, possibly accompanied by additive-assisted grain coarsening{*Nat. Commun.* 2025, *16*, 10456}.

This interpretation is further supported by our ^{207}Pb solid-state NMR experiments (see **Figure R19 a,b**), which were performed on a fully phase-separated $MAPbI_3$/$MAPbBr_3$ powder mixture, thereby excluding the contribution from the initial halide-mixing differences in the wet-film stage. The ^{207}Pb solid-state NMR spectra track the evolution of Pb coordination environments from segregated I-rich and Br-rich phase toward mixed [$PbI_{6-x}Br_x$] phase during thermal treatment, thus serving as a direct probe for the halide ion mobility across grains under thermal activation {*ACS Energy Lett.* 2023, *8*, 5041−5049}. Compared with the control, the TDB-treated sample evolved much faster toward the intermediate chemical-shift regime, indicating that TDB significantly promotes faster halide mixing by accelerating the halide migration kinetics across grain boundaries under thermal activation. the TDB-treated sample appeared much darker after 4 h of thermal treatment, approaching the color of the mixed-halide phase, whereas the control sample still retained an orange hue, indicative of residual Br-rich phase (see **Figure 19c**).

We have added the discussion in the revised manuscript on p.7: "Secondly, during annealing, the TDB-treated film showed much faster halide-mixing kinetics than the control and ultimately evolved into a single diffraction peak (**Fig. 1g,h**), partly owing to the homogeneous phase distribution in the wet-film state. In addition, additive-assisted grain coarsening also contributes to the final halide homogenization. To further probe this process, we performed ^{207}Pb solid-state NMR experiments on a fully separated $MAPbI_3$ and $MAPbBr_3$ powder mixture[22,23] (**Fig. 1l**). The ^{207}Pb solid-state NMR is highly sensitive to the local coordination environment of Pb centers in [PbX_6] octahedra. During halide mixing, the progressive exchange between I^- and Br^- continuously alters the local Pb–X configuration toward mixed [$PbI_{6-x}Br_x$] octahedra, leading to characteristic changes in the ^{207}Pb chemical shift. Therefore, the evolution of the ^{207}Pb NMR spectra directly reflects the evolution from segregated I-rich and Br-rich phases to a mixed-halide state during thermal treatment. Compared with the control, the TDB-treated sample evolved much faster toward a mixed-halide chemical environment, indicating accelerated thermally driven halide mixing. This effect may originate from the ability of TDB to facilitate ion transport[22,23]. Consistent with this result, the TDB-treated sample displayed a color closer to that of the mixed-halide phase, whereas the control sample still retained an orange hue, indicative of residual Br-rich domains (Supplementary Fig. 6)."

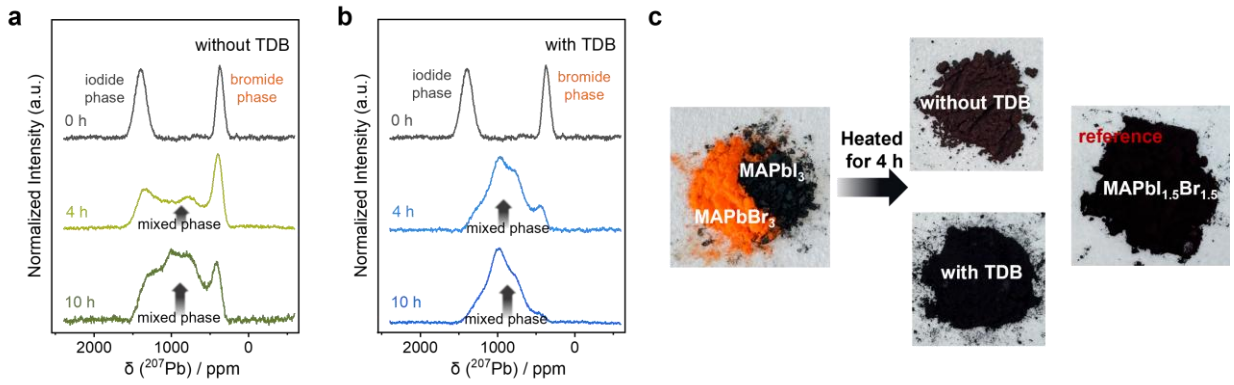

Figure R19 (**Figure 1l** and **Supplementary Figure 6**). **a,b,** ^{207}Pb solid-state NMR spectra of perovskite powders without TDB and with TDB after thermal treatment for different durations. **c,** Photographs of the powder samples used for ^{207}Pb solid-state NMR characterization showing the changes in $MAPbI_3$ and $MAPbBr_3$ powders without and with TDB after mixing in the dark at 80 °C for 4 h.

To understand why TDB accelerates halide mixing during annealing, we used its photo-converted product TAB (Supplementary Fig. 4) for comparison and inferred that TDB can effectively promote thermally activated halide migration through an "ion-shuttle-like" mechanism {*ACS Energy Lett.* 2023, *8*, 5041–5049}, involving the capture, transport, and exchange of halide ions. Liquid-state NMR revealed electrostatic interactions between TDB and halide anions (Supplementary Fig. 3b). DFT calculations (see **Table R2**) further showed that both TDB and TAB interact with halide ions much more strongly than solvent molecules, suggesting that both molecules can act as halide-ion capturing species to facilitate the migration of halide ions {*Nat. Commun.* 2025, *16*, 9894}. Meanwhile, UPS (see **Figure R20**) supports pronounced electronic interactions between TDB/TAB and the local lead–halide framework, indicating that both molecules can participate in the ion-exchange environment near the perovskite surface. Moreover, DFT calculations (see **Table R3**) show that TDB has a lower desorption energy from the perovskite surface than TAB, which is consistent with the steric hindrance introduced by its rigid three-membered diazirine ring, as well as the stronger lone-pair coordination between the oxygen atom in TAB and surface Pb sites, allowing TDB to detach more readily from surface sites under thermal activation and to enable more effective halide ion transport. In contrast, the stronger surface binding of TAB is expected to hinder this dynamic process. To further support this interpretation, we performed ^{207}Pb solid-state NMR measurements using TAB as a comparison (see **Figure R21**) which showed that TAB is much less effective than TDB in promoting halide mixing during thermal treatment, further supporting the more effective "ion-shuttle-like" role of TDB in accelerating halide mixing.

We have added Supplementary Fig. 29 in SI

We have added Supplementary Fig. 37 in SI

We have added Supplementary Table. 1 in SI

We have added Supplementary Table. 4 in SI

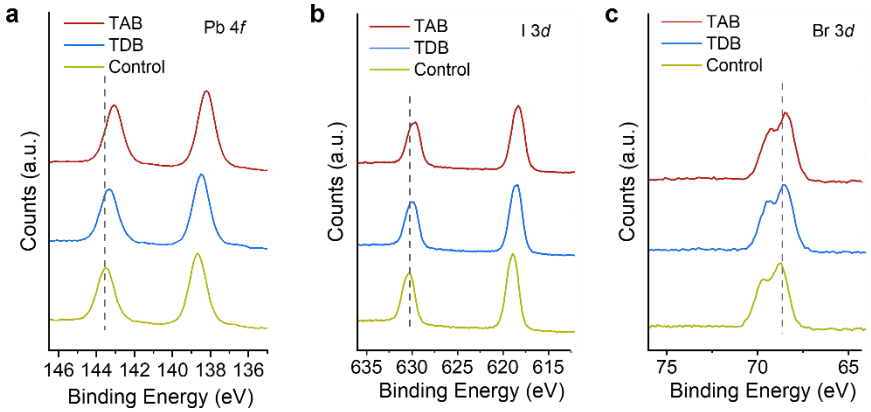

Figure R20 (Supplementary Figure 29). X-ray photoelectron spectroscopy (XPS) spectrum of Pb 4*f*, I 3*d and* Br 3*d* in the perovskite films without or with TAB and TDB treatment.

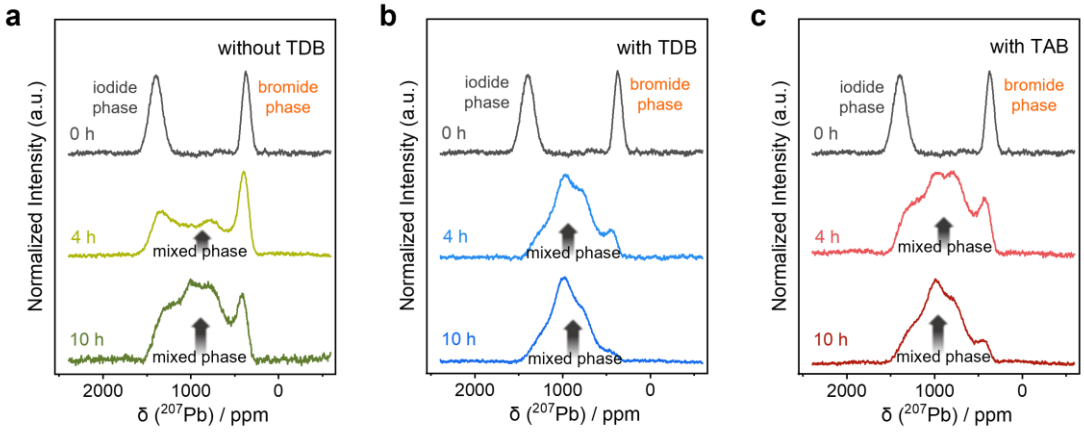

Figure R21 (Supplementary Figure 37). ^{207}Pb solid-state NMR spectra of perovskite powders without TDB, with TDB, and with TAB after thermal treatment for different durations. The initial spectra at 0 h show distinct signals assigned to the iodide-rich and bromide-rich phases. Upon thermal treatment, the spectra gradually evolve toward the intermediate chemical-shift region, indicating progressive halide intermixing and the formation of mixed-halide local environments.

Table R2 (Supplementary Table 4). Calculated binding energies between different molecules and I^-/Br^- ions.

Species	I^-	Br^-
DMF	−0.5309	−0.6504
DMSO	−0.6780	−0.8193
TAB	−4.8602	−5.2180
TDB	−4.7525	−5.1680

Table R3 (Supplementary Table 4). The maximum and minimum points (φ_{max} and φ_{min}) of the electrostatic potential and adsorption energy of TAB and TDB.

molecule	φ_{max} (kcal/mol)	φ_{min}(kcal/mol)	adsorption energies
TAB	158.1	31.1	-8.2 eV
TDB	154.8	33.4	-6.9 eV

To evaluate the effect of TDB on the crystalline quality of perovskite films, we extracted GIWAXS patterns from the *in-situ* measurements at the end of annealing, which reveal a strong out-of-plane preferred orientation in the TDB-treated film (see **Fig. R22**). To understand how this orientational ordering develops, we tracked the azimuthal angular intensity of the perovskite (100) diffraction signal (around q = 1 $Å^{-1}$) as a function of annealing time (see **Fig. R23**). Before heating, both films exhibited similarly broad angular distributions, whereas after annealing started, the TDB-treated film showed a clear azimuthal redistribution with the scattering intensity progressively concentrated near 0°, while the control film remained broadly distributed around ~45°. These results indicate that TDB mainly promotes crystallite reorientation and orientational ordering during thermal annealing.

We have added Figure 1m in main text.

We have added Supplementary Fig. 9 in SI.

We have added the discussion in the revised manuscript on p.8: "GIWAXS patterns extracted from the *in-situ* measurements at the end of annealing further reveal a strong out-of-plane preferred orientation in the TDB-treated film (**Fig. 1m**). Distinct PbI_2 diffraction and non-photovoltaic δ-phase were also found in the control perovskite film, but were absent in the target perovskite film, suggesting suppressed local compositional inhomogeneity, which is consistent with more thorough halide mixing. To understand the development of orientational ordering, we tracked the azimuthal angular intensity of the perovskite (100) diffraction signal (around q = 1

Å^{-1}) during annealing (Supplementary Fig. 9), indicating that TDB promotes crystallite reorientation and orientational ordering during thermal annealing[23].”

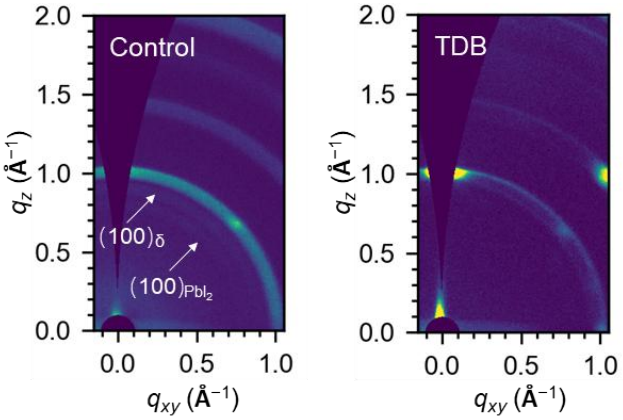

Figure R22 (**Figure 1m**)**.** GIWAXS images of the perovskite films without and with TDB treatment extracted from the *in-situ* measurements at the end of annealing.

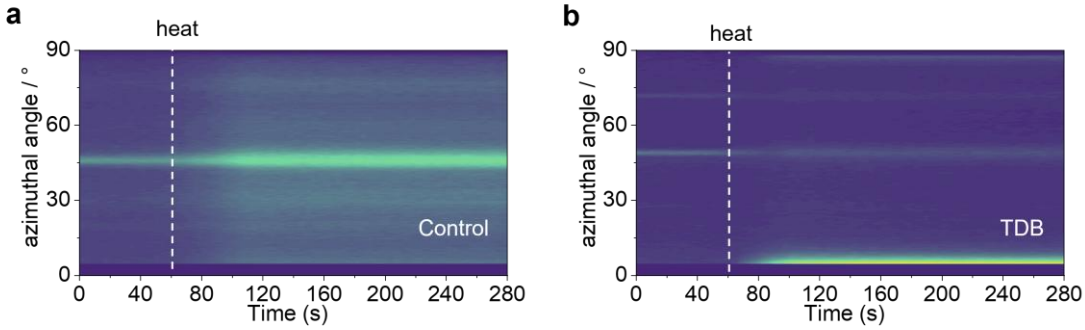

Figure R23 (**Supplementary Figure 9**). Azimuthal angular intensity of the perovskite diffraction signal as a function of time for the control and TDB-treated films during annealing.

Taken together, I believe that the findings of the authors can be suitable to be published in nature, if the manuscript is able to clarify the working mechanism of the additive both for reduced halides segregation and crystallization and further the authors can provide a certificate with proper measurement procedure (which would then also enter one of the well-known efficiency lists).

Comments from Reviewer 2 and replies from the authors

This article demonstrates an interesting additive approach using the photo-transformable 4-[3-(trifluoromethyl)-3H-diazirin-3-yl]benzylamine hydrochloride (TDB) to retard halide segregation in wide-bandgap perovskites, achieving a certified 28.02% perovskite–organic tandem efficiency. The efficiency is quite remarkable; however, several critical concerns should be resolved before this article can be published in Nature.

1. (Originality)

The authors used 4-[3-(trifluoromethyl)-3H-diazirin-3-yl]benzylamine hydrochloride to suppress halide segregation and passivate point defects in perovskite materials. However, another group recently reported modulation of carrier dynamics and improvement of perovskite film quality and stability using 4-(3-(trifluoromethyl)-3H-diazirin-3-yl)benzylamine, which has exactly the same structure except for the presence of the HCl salt (Yang et al., Journal of Alloys and Compounds, 2025, 1048, 185243). Both molecules contain the same functional groups except for protonation, which means that the basic conceptual strategy for improving photovoltaic performance is quite similar. The authors should address this originality issue.

Response: We appreciate the reviewer's comment and the opportunity to clarify the originality of our work. We carefully studied the paper by Yang et al. (*Journal of Alloys and Compounds*, 2025, *1048*, 185243), and for clarity, we have displayed the molecular structure in **Fig. R24**. We will discuss the originality of our work from two perspectives: the distinct molecular structure of TDB and its functional mechanism.

(1). The molecule reported in that work, 4-(trifluoromethyl)benzohydrazine, belongs to the **acylhydrazine** family. We agree that it shares some structural similarities with the additive TDB used in our study, like the trifluoromethyl group and phenyl backbone, but the two compounds are different in their core functional groups and chemical properties.

(2). TDB contains a unique **trifluoromethyl diazirine moiety**, which gives it a photo-transformable character, meanwhile, while its hydrochloride form enables electrostatic interaction with the halide. These features suggest a working mechanism that is different from that in the cited work, where 4-(trifluoromethyl)benzohydrazine mainly improves Sn–Pb perovskite film crystallinity and carrier dynamics through coordination and hydrogen-bonding interactions. Our work is focus on suppressing halide segregation in WBG perovskites across both the halide-mixing stage and the subsequent device operation stage under illumination.

We hope that our response has adequately clarified this issue and addressed the reviewer's concern.

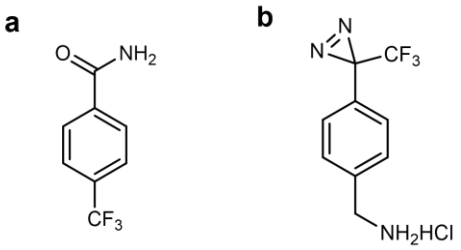

Figure. R24. Comparison of the molecular structures 4-(trifluoromethyl)benzohydrazine discussed in the cited work (**a**), and TDB used in this work (**b**).

2. (Science)

Many photo-responsive and redox-active additives have been reported for stabilizing halide perovskites. For example, photochromic molecules in their open form (after illumination) have been shown to bond with perovskite materials and passivate point defects. In the case of TDB, what is the fundamental science that differs from previously reported photoactive passivation molecules? The authors need to clarify the special interaction between the functional groups and wide-bandgap halide perovskites from a scientific perspective (not only through simple bonding-energy simulations). Why is this TDB molecule particularly effective at suppressing halide-ion segregation? What is the rule of thumb?

Response: We appreciate the reviewer's comment. In the revised manuscript, we propose **a two-stage strategy** enabled by the **photo-transformable property** of TDB to suppress halide segregation in high-Br-content WBG perovskites.

First, during the crystallization stage, TDB **promoting more homogeneous halide mixing** in the as-formed perovskite film. This view is supported by multiple lines of evidence, including *in situ* GIWAXS, solid-state ^{207}Pb NMR and DFT calculations.

Second, during operation under illumination, TDB undergoes photo-conversion to form TAB. TAB possesses a larger dipole moment and stronger adsorption on the perovskite surface than TDB, and therefore no longer acts as a dynamic mediator for halide mixing. Instead, owing to its stronger anchoring at surface defect sites, TAB increases the formation energies of iodine vacancies and iodine interstitials which are key defects involved in halide migration, thereby **suppressing defect-assisted halide de-mixing**.

We have added the discussion in the revised manuscript in p.2: "Here, we introduced a photo-transformable additive 4-[3-(trifluoromethyl)-3H-diazirin-3-yl]benzylamine (TDB) into the WBG perovskite precursor solution to establish a two-stage strategy for stabilizing the mixed-halide phase. During crystallization, TDB initial halide homogeneity by suppressing the rapid precipitation of the Br-rich phase in the wet film and accelerating halide mixing during annealing; during operation under illumination, TDB undergoes transformation to form a new species with stronger adsorption on the perovskite surface, which inhibits the formation of iodide related defects, suppresses defect-assisted carrier trapping and ion migration and thereby mitigates light-induced halide segregation[9,10]."

We have added the discussion in the revised manuscript in p.3: "Here we introduced 4-[3-(trifluoromethyl)-3H-diazirin-3-yl]benzylamine (TDB), an aromatic ammonium cation with deliberately designed functional groups, into the WBG perovskite precursor solution. During crystallization, TDB features a three-membered diazirine engages in multisite interactions with FAI and lead halides, thereby suppressing the rapid precipitation of the Br-rich phase in the wet film. This wet-film state with homogeneous phase distribution provides a foundation for halide

mixing during annealing, thereby improving the halide homogeneity of the final film."

We have also added the discussion in the revised manuscript in p.4: "The newly generated TAB with higher dipole moment exhibits stronger adsorption on the perovskite surface and increases the formation energy of iodine-related defects, thereby suppressing defect-assisted carrier trapped and halide-ion migration, consequently enhances the photo-stability of the WBG perovskite."

In the following, we address the reviewer's question from the two-stage strategy enabled by the photo-transformable property of TDB.

***(1)*. During the crystallization stage**

We devoted efforts to design an *in situ* GIWAXS sample chamber equipped with a spin coater and an antisolvent syringe under a N_2 atmosphere, allowing recording the **full process from spin-coating to annealing.** As shown in **Fig. R25**, the wet films exhibited a single diffraction peak immediately after antisolvent dripping. However, once spinning stopped, this initially single peak immediately split into two distinct peaks corresponding to Br-rich and I-rich phases (see **Fig. R25b**), indicating that the reduced solvent evaporation rate after spinning amplified the solubility disparity between the two phases. A similar phenomenon was also observed in the *in situ* PL measurements during spin-coating (see **Fig. R26**). During annealing, the diffraction peak of the control sample broadened at the early stage, indicating the onset of halide mixing together with local variations in unit-cell size{*Energy Environ. Sci.* 2025, *18*, 10460–10472}. With prolonged annealing, the peak gradually narrowed and shifted toward lower *q* values, reflecting the gradual incorporation of iodide into the perovskite lattice. Nevertheless, the control sample exhibited slow mixing kinetics and did not evolve into a homogeneous mixed-halide phase within the annealing time (see **Fig. R25c,d**).

To improve the initial halide homogeneity of the WBG perovskite, we introduced TDB (Supplementary Fig. 3a) into the precursor solution. Although some peak broadening was also observed in the TDB-treated wet film after spinning, the diffraction feature could still be mainly assigned to a mixed-halide phase, with only minor variation (see **Fig. R25e,f**). During annealing, the TDB-treated film showed much faster halide-mixing kinetics than the control and ultimately evolved into a single diffraction peak, indicative of a more homogeneous mixed-halide phase (see **Fig. R25g,h**).

We have added Supplementary Fig. 2 in SI

We have added the discussion in the revised manuscript on p.4: "Firstly, during spin-coating (**Fig. 1a**), the wet films of control sample exhibited a single diffraction peak after antisolvent dripping without detectable δ phase or solvent-associated intermediate phase. Once spinning stopped, this single peak immediately split into two distinct peaks (**Fig. 1b**), indicating clear phase separation. A similar transition was also observed in the *in situ* PL measurements (Supplementary

Fig. 2). We infer that the slower solvent evaporation after spinning amplified the solubility disparity between the Br-rich and I-rich phases, while the faster crystallization of the Br-rich phase further promoted its precipitation. Secondly, during annealing (**Fig. 1c**), the phase separation inherited from the wet-film persisted. Then, the diffraction peak of the film broadened, which indicated the onset of halide mixing[21] and gradually narrowed with prolonged annealing. Nevertheless, the diffraction peak of the control sample remained noticeably broadened (**Fig. 1d**) rather than evolving into a sharp single peak characteristic, indicating incomplete halide homogenization."

We have added the discussion in the revised manuscript on p.5: "To investigate how TDB influenced the crystallization of high-Br-content WBG perovskite, we introduced TDB into the precursor solution and monitored the crystallization process by *in situ* GIWAXS. Firstly, the spin-coating process was shown in **Fig. 1e**, although some peak broadening was observed in the TDB-treated wet film after spinning, the diffraction feature could still be mainly assigned to a mixed-halide phase, with only minor variation (**Fig. 1f**), indicating the TDB-treated wet film retains a stabilized mixed-halide phase without obvious segregation, which arise from the interactions of TDB with FA and lead halides, enabled by the two electron-rich N atoms in the diazirine unit. These interactions help suppress the rapid precipitation of the Br-rich phase, thereby stabilizing the mixed-halide phase during spin-coating process. This wet-film state with homogeneous phase distribution provides a foundation for halide mixing during annealing, thereby contributing to the improved halide homogeneity of the final film."

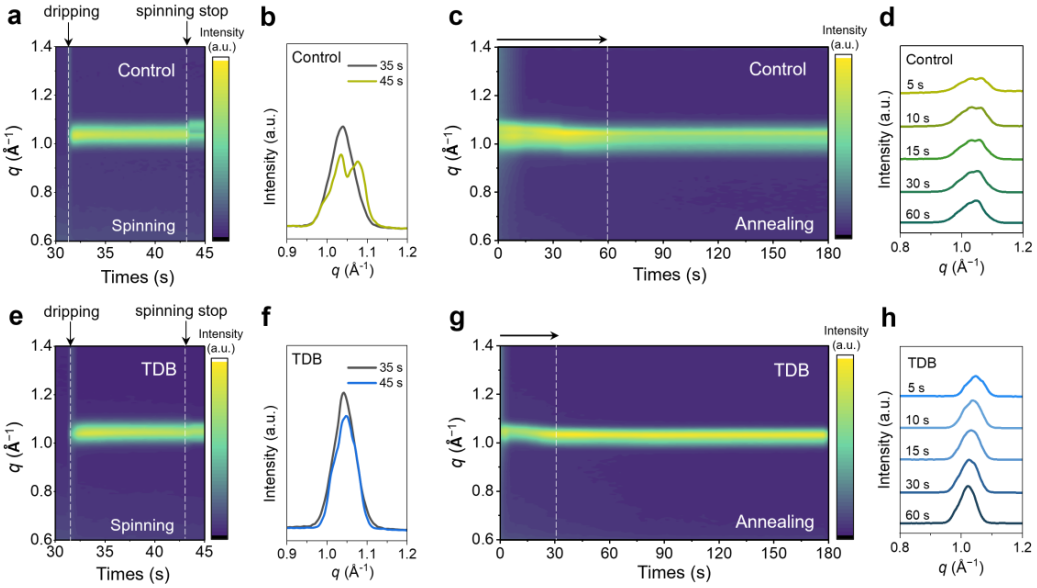

Figure R25 (Figure 1a-h). *In situ* GIWAXS patterns recorded during the spin-coating of wet perovskite films ($FA_{0.8}Cs_{0.2}Pb(I_{0.5}Br_{0.5})_3$) without and with TDB treatment. Antisolvent dripped at 31 s; spin-coating stopped at 43 s.

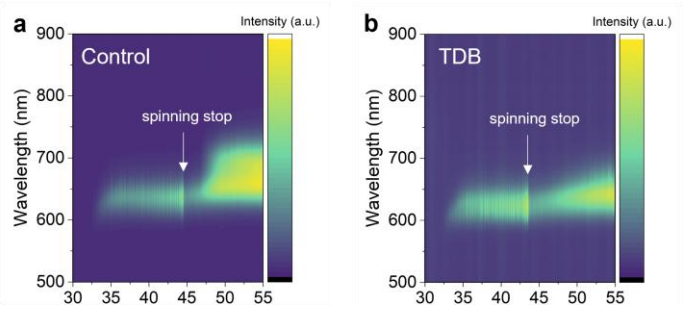

Figure R26 (Supplementary Figure 2) *In situ* PL characterization of phase evolution in control and TDB-treated WBG perovskite films during spin-coating.

The TDB-treated 50 mol% Br WBG perovskites exhibited less pronounced phase separation both in the wet-film state and the final film. The weaker phase separation in the TDB-treated wet film may arise from the interaction between TDB and FA^+, which could retard crystallization{s41560-026-02010-z} and narrow the kinetic disparity between the precipitation of the Br-rich and I-rich phases (Supplementary Fig. 3), but this effect is unlikely to be the dominant origin of the improved final halide mixing. Instead, the halide mixing during annealing is more likely governed by a reorganization of the pre-existing crystal structure, possibly accompanied by additive-assisted grain coarsening{*Nat. Commun.* 2025, *16*, 10456}.

This interpretation is further supported by our ^{207}Pb solid-state NMR experiments (see **Figure R27a,b**), which were performed on a fully phase-separated $MAPbI_3$/$MAPbBr_3$ powder mixture, thereby excluding the contribution from the initial halide-mixing differences in the wet-film stage. The ^{207}Pb solid-state NMR spectra track the evolution of Pb coordination environments from segregated I-rich and Br-rich phase toward mixed [$PbI_{6-x}Br_x$] phase during thermal treatment, thus serving as a direct probe for the halide ion mobility across grains under thermal activation {*ACS Energy Lett.* 2023, *8*, 5041−5049}. Compared with the control, the TDB-treated sample evolved much faster toward the intermediate chemical-shift regime, indicating that TDB significantly promotes faster halide mixing by accelerating the halide migration kinetics across grain boundaries under thermal activation. the TDB-treated sample appeared much darker after 4 h of thermal treatment, approaching the color of the mixed-halide phase, whereas the control sample still retained an orange hue, indicative of residual Br-rich phase (see **Figure 27c**).

We have added the discussion in the revised manuscript on p.7: "Secondly, during annealing, the TDB-treated film showed much faster halide-mixing kinetics than the control and ultimately evolved into a single diffraction peak (**Fig. 1g,h**), partly owing to the homogeneous phase distribution in the wet-film state. In addition, additive-assisted grain coarsening also contributes to the final halide homogenization. To further probe this process, we performed ^{207}Pb solid-state NMR experiments on a fully separated $MAPbI_3$ and $MAPbBr_3$ powder mixture[22,23] (**Fig. 1l**). The

^{207}Pb solid-state NMR is highly sensitive to the local coordination environment of Pb centers in [PbX_6] octahedra. During halide mixing, the progressive exchange between I^- and Br^- continuously alters the local Pb–X configuration toward mixed [$PbI_{6-x}Br_x$] octahedra, leading to characteristic changes in the ^{207}Pb chemical shift. Therefore, the evolution of the ^{207}Pb NMR spectra directly reflects the evolution from segregated I-rich and Br-rich phases to a mixed-halide state during thermal treatment. Compared with the control, the TDB-treated sample evolved much faster toward a mixed-halide chemical environment, indicating accelerated thermally driven halide mixing. This effect may originate from the ability of TDB to facilitate ion transport[22,23]. Consistent with this result, the TDB-treated sample displayed a color closer to that of the mixed-halide phase, whereas the control sample still retained an orange hue, indicative of residual Br-rich domains (Supplementary Fig. 6).”

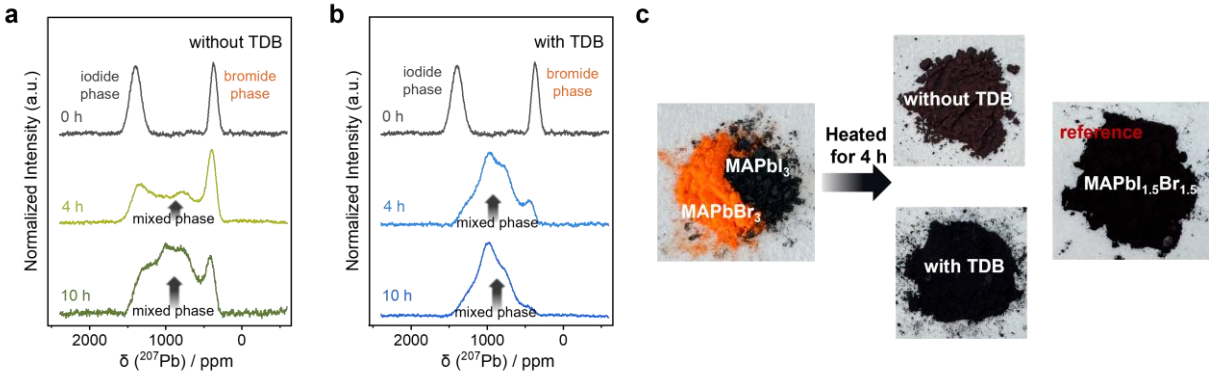

Figure R27 (**Figure 1l** and **Supplementary Figure 6**). **a,b,** ^{207}Pb solid-state NMR spectra of perovskite powders without TDB and with TDB after thermal treatment for different durations. **c**, Photographs of the powder samples used for ^{207}Pb solid-state NMR characterization showing the changes in $MAPbI_3$ and $MAPbBr_3$ powders without and with TDB after mixing in the dark at 80 °C for 4 h.

To understand why TDB accelerates halide mixing during annealing, we used its photo-converted product TAB (Supplementary Fig. 4) for comparison and inferred that TDB can effectively promote thermally activated halide migration through an “ion-shuttle-like” mechanism {*ACS Energy Lett.* 2023, *8*, 5041–5049}, involving the capture, transport, and exchange of halide ions. Liquid-state NMR revealed electrostatic interactions between TDB and halide anions (Supplementary Fig. 3b). DFT calculations (see **Table R4**) further showed that both TDB and TAB interact with halide ions much more strongly than solvent molecules, suggesting that both molecules can act as halide-ion capturing species to facilitate the migration of halide ions {*Nat.*

Commun. 2025, *16*, 9894}. Meanwhile, UPS (see **Fig. R28**) supports pronounced electronic interactions between TDB/TAB and the local lead–halide framework, indicating that both molecules can participate in the ion-exchange environment near the perovskite surface. Moreover, DFT calculations (see **Table R5**) show that TDB has a lower desorption energy from the perovskite surface than TAB, allowing TDB to detach more readily from surface sites under thermal activation and to enable more effective halide ion transport. In contrast, the stronger surface binding of TAB is expected to hinder this dynamic process. To further support this interpretation, we performed ^{207}Pb solid-state NMR measurements using TAB as a comparison (see **Fig. R29**) which showed that TAB is much less effective than TDB in promoting halide mixing during thermal treatment, further supporting the more effective "ion-shuttle-like" role of TDB in accelerating halide mixing.

We have added Supplementary Fig. 29 in SI

We have added Supplementary Fig. 37 in SI

We have added Supplementary Table. 1 in SI

We have added Supplementary Table. 4 in SI

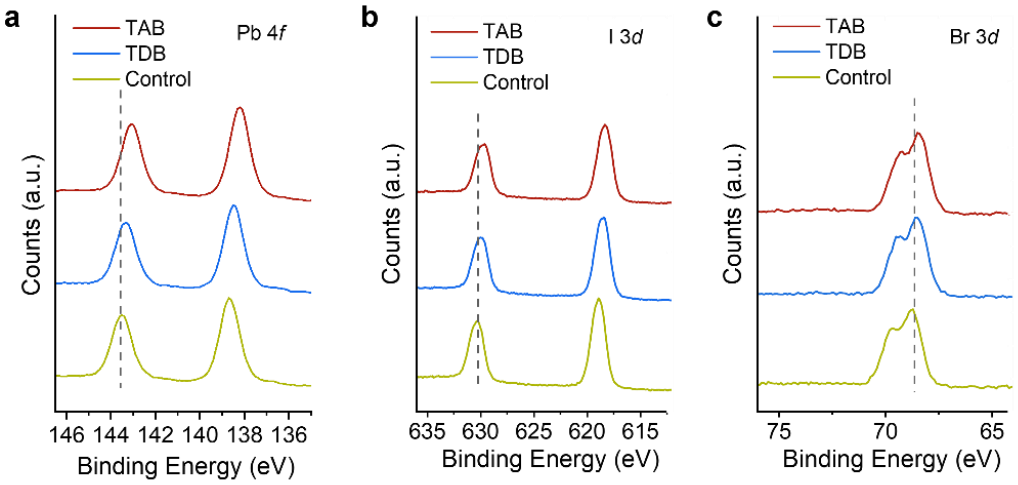

Figure R28 (Supplementary Figure 29). X-ray photoelectron spectroscopy (XPS) spectrum of Pb 4*f*, I 3*d and* Br 3*d* in the perovskite films without or with TAB and TDB treatment.

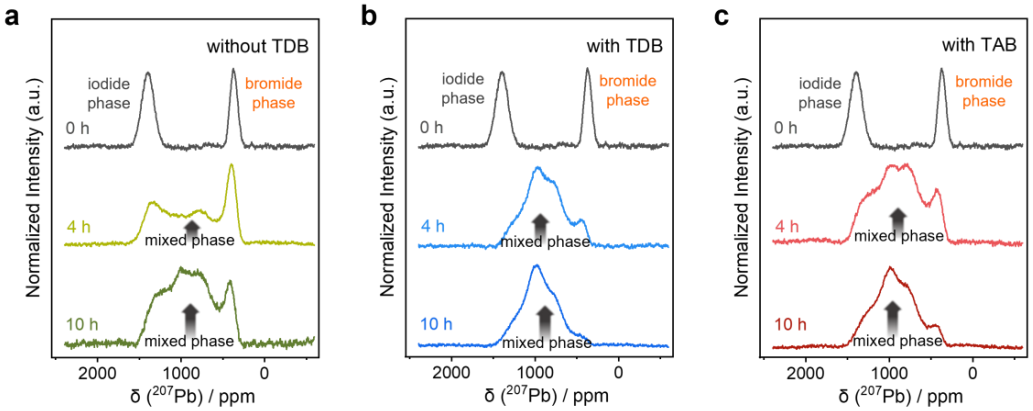

Figure R29 (Supplementary Figure 37). ^{207}Pb solid-state NMR spectra of perovskite powders without TDB, with TDB, and with TAB after thermal treatment for different durations. The initial spectra at 0 h show distinct signals assigned to the iodide-rich and bromide-rich phases. Upon thermal treatment, the spectra gradually evolve toward the intermediate chemical-shift region, indicating progressive halide intermixing and the formation of mixed-halide local environments.

Table R4 (Supplementary Table 1). Calculated binding energies between different molecules and I^-/Br^- ions

Species	I^-	Br^-
DMF	−0.5309	−0.6504
DMSO	−0.6780	−0.8193
TAB	−4.8602	−5.2180
TDB	−4.7525	−5.1680

Table R5 (Supplementary Table 4). The maximum and minimum points (φ_{max} and φ_{min}) of the electrostatic potential and adsorption energy of TAB and TDB.

molecule	φ_{max} (kcal/mol)	φ_{min}(kcal/mol)	adsorption energies
TAB	158.1	31.1	-8.2 eV
TDB	154.8	33.4	-6.9 eV

***(2)*. During operation under illumination**

Owing to the photo-transformable nature of TDB, reactions occur under illumination and

generate new species, we called this TAB. We employed ^{19}F NMR as an analytical tool to provide direct and quantitative evidence for the TDB-to-TAB conversion in perovskite film (**Fig. R36**).

We have added Supplementary Fig. 28 in SI

We have added discussion in p.12: "We employed ^{19}F NMR as an analytical tool to provide direct and quantitative evidence for the TDB-to-TAB conversion in perovskite film (Supplementary Fig. 28)."

The electron-withdrawing carbonyl group in TAB increases the maximum electrostatic potential on the ammonium side while lowering the minimum electrostatic potential on the opposite side, thereby giving TAB a larger dipole moment than TDB (see **Fig. R30a,b,** and **Table R5**). This enlarged dipole strengthens the electrostatic interaction between the ammonium group and the perovskite surface. In addition, the carbonyl oxygen can further coordinate with undercoordinated Pb sites, giving rise to a multisite anchor mode. DFT calculations reveal that TAB exhibits a shorter binding distance and stronger adsorption on the perovskite surface than TDB (see **Fig. R30c,d,** and **Table R5**). More importantly, TAB treatment increases the formation energies of iodine vacancies and iodine interstitials (see **Fig. R31**). The suppression of these iodide-related defects mitigates defect-assisted carrier trapping, which is expected to reduce the free-energy gain of the de-mixing state. Meanwhile, the reduced defect density also inhibits defect-mediated halide-ion migration, thereby suppressing phase segregation under illumination.

We have added Supplementary Fig. 30 in SI.

We have added the discussion in the revised manuscript in p.12: "DFT calculations indicate that TAB possesses a larger dipole moment (**Fig. 3b**) and stronger adsorption on the perovskite surface than TDB (**Fig. 3c,d** and data is shown in Supplementary Table. 4), owing to its multisite anchoring mode involving electrostatic interaction through the ammonium group together with additional coordination of the carbonyl oxygen to undercoordinated Pb sites. X-ray photoelectron spectroscopy (XPS) measurements also demonstrated these results (Supplementary Fig. 29). Moreover, TAB increases the formation energies of iodine vacancies and iodine interstitials (Supplementary Fig. 30)."

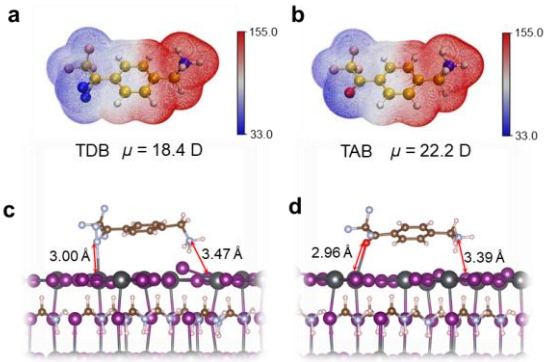

Figure R30 (Figure 3b-d). Electrostatic potential surfaces of (**a**) TDB and (**b**) TAB. Calculated adsorption models of (**c**) TDB and (**d**) TAB on the perovskite surface.

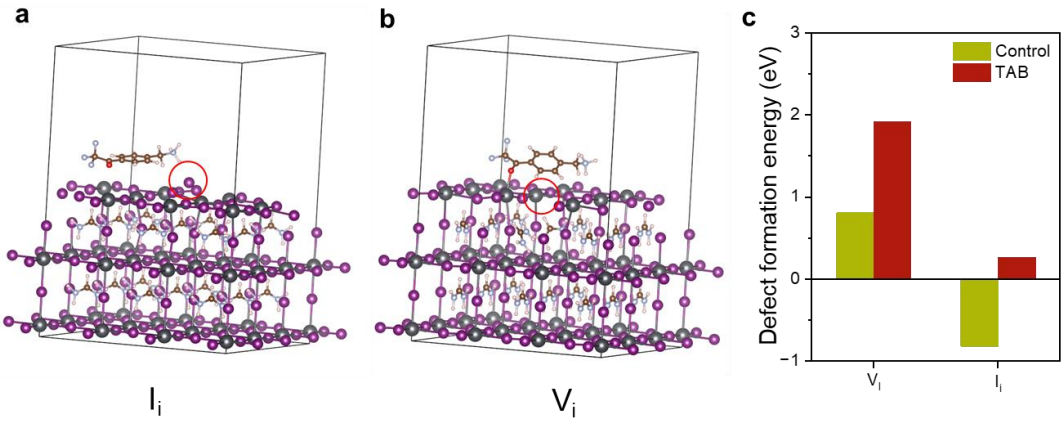

Figure R31 (**Supplementary Figure. 30**). **a,b,** Optimized tructures of TAB adsorbed on the perovskite surface with iodide interstitial and iodide vacancy, respectively. **c,** Calculated formation energies of V_I and I_i of the control and TAB-treated perovskites.

We performed Transient photocurrent (TPC) measurements (see **Figure R32**) to confirm the inhibited defect-assisted carrier trapping. The shortest decay time observed for the TAB-treated device suggests reduced defect-assisted carrier trapping and charge accumulation.

We have added the discussion in the revised manuscript in p.12: "The suppression of these iodide-related defects mitigates defect-assisted carrier trapping. Transient photocurrent (TPC) measurements (Supplementary Figure. 31) were performed on the control, TDB-treated, and TAB-treated pero-SCs. The shortest decay time observed for the TAB-treated device suggests reduced defect-assisted carrier trapping and charge accumulation[36]. Meanwhile, the reduced defect density also suppresses defect-mediated halide-ion migration[37]."

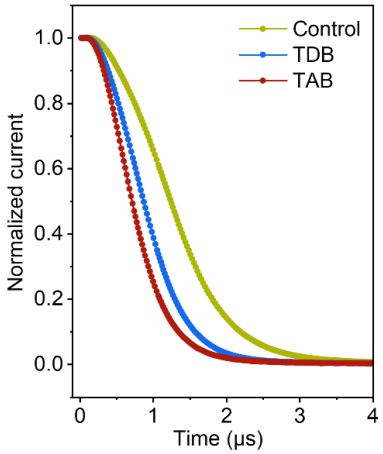

Figure R32 (Supplementary Figure 31). Transient photocurrent (TPC) measurements for the control, TDB-treated, and TAB-treated pero-SC devices. The normalized TPC decay curves were fitted with a single-exponential function, yielding characteristic decay times of approximately 1.10, 0.86, and 0.68 μs, respectively.

We performed continuous-illumination PL measurements to directly confirm that TAB suppresses light-induced phase segregation effectively (see **Figure R33**). We prepared control, TAB-treated, and TDB-treated perovskite films, in which TAB or TDB was spin-coated from IPA solution onto pristine perovskite films as a surface treatment. Under continuous 1-sun illumination, the control film developed an additional emission peak at ~740 nm, assigned to an I-rich phase, which dominated the spectrum after 20 min. In contrast, the TAB-treated film showed a much lower extent of halide segregation, with almost no red-shifted peak observed throughout the measurement. Although TDB treatment also showed a certain ability to suppress phase segregation, its effect was clearly less pronounced than that of TAB. This trend is further supported by the evolution of the I-rich-to-intrinsic peak ratio and is consistent with the above theoretical analysis.

We have added the discussion in the revised manuscript in p.13: "Continuous-illumination PL measurements were performed to directly verify the role of TAB in suppressing phase segregation (**Figs. 3e-g**). While the control film developed a pronounced red-shifted emission at ~740 nm, assigned to an I-rich phase, the TAB-treated film showed almost no such peak throughout the measurement. Although TDB treatment also showed a certain ability to suppress phase segregation, its effect was clearly less pronounced than that of TAB. This trend is further supported by the evolution of the I-rich-to-intrinsic peak ratio (Supplementary Fig. 33) and is consistent with the above theoretical analysis."

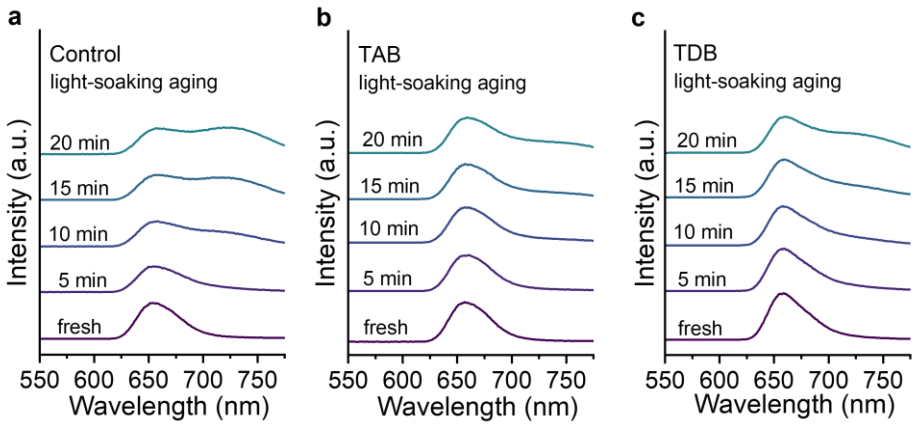

Figure R33. (**Figures. 3e-g**) PL evolution for control, TAB and TDB treated perovskite films after light soaking under 1-sun illumination for 20 minutes.

Furthermore, we compared the scan-rate-dependent J_{sc} of devices measured before and after aging (see **Figure R34**). Even in the fresh state, the target devices already showed weaker scan-rate dependence than the control devices, indicating reduced ionic losses in the initially formed

devices, which is consistent with the role of TDB in promoting more homogeneous halide mixing during film formation. After 24 h of aging, this contrast became even more pronounced, with the control devices exhibiting much stronger scan-rate dependence, indicating more severe ion-related losses that are consistent with increasing phase segregation during operation. This device-level behavior further supports the synergistic roles of TDB in improving the initial halide homogeneity and TAB in suppressing defect-assisted halide de-mixing under illumination.

We have added the discussion in the revised manuscript in p.13: "Furthermore, we compared the scan-rate-dependent J_{sc} of devices measured before and after aging (**Figs. 3h,i**). Even in the fresh state, the target devices already showed weaker scan-rate dependence than the control devices, indicating reduced ionic losses in the initially formed devices, which is consistent with the role of TDB in promoting more homogeneous halide mixing during film formation. After 12 h of aging, this contrast became even more pronounced, with the control devices exhibiting much stronger scan-rate dependence, indicating more severe ion-related losses that are consistent with increasing phase segregation during operation[20]. This behavior further supports the synergistic roles of TDB in improving the initial halide homogeneity and TAB in suppressing defect-assisted halide de-mixing under illumination."

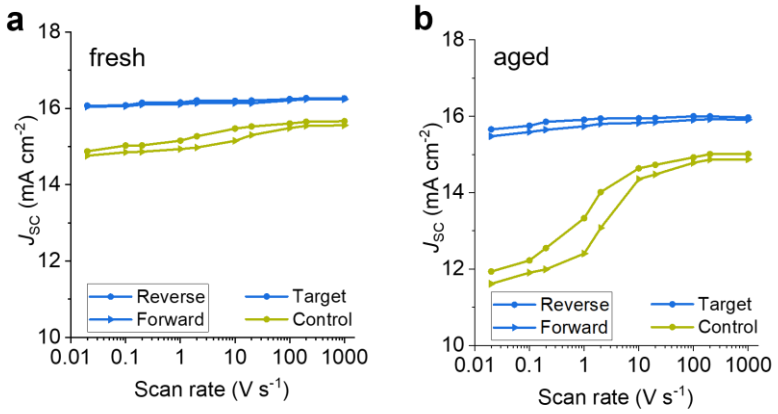

Figure R34 (**Figures. 3h,i**) Comparison of the scan-rate-dependent J_{sc} of control and target WBG pero-SCs before (**a**) and after aging (**b**).

To assess the phase separation in the WBG front-cell after aging in the integrated tandem architecture, we measured the electroluminescence (EL) characteristics of the control and target perovskite–organic TSCs after aging under ISOS-L-1 protocol (see **Fig. R35)** The aged control device exhibited an additional emission peak at ~740 nm, assigned to an I-rich phase, across different injection current densities, indicating pronounced phase segregation after light-soaking aging. By contrast, the EL peak of the WBG front cell in the target device retained its position with increasing injection current density. These results indicate that the target device remains more resistant to bias-induced phase segregation even after light-soaking aging.

We have added the discussion in the revised manuscript on p.15: "We measured the EL spectra of the control and target perovskite–organic TSCs after 240 h of ISOS-L-1 aging to probe phase segregation of the WBG front cell in aged integrated tandem devices (**Fig. 4e,f**). The aged control device exhibited an additional emission peak at ~740 nm across different injection current densities, which is assigned to an I-rich phase. However, the target device retained a stable EL peak position indicating that the target device remains more resistant to bias-induced phase segregation even after light-soaking aging[42]."

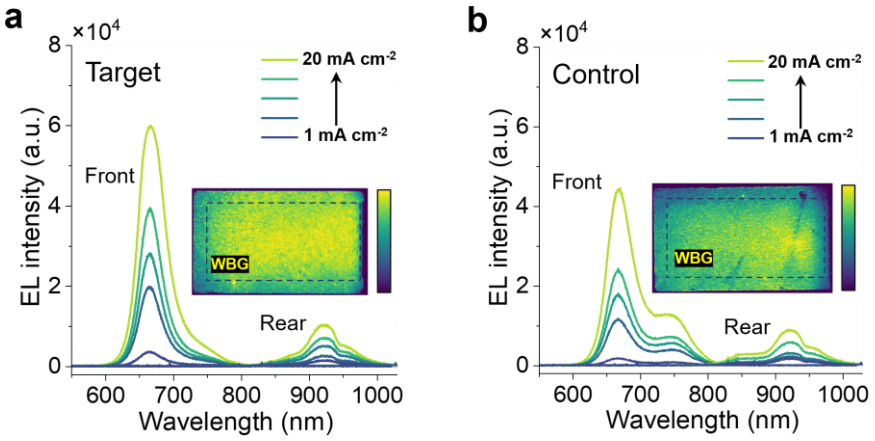

Figure. R35 (**Figures. 4e,f**). EL spectra of the aged (**a**) control and (**b**) target perovskite–organic TSCs measured at different injection current densities for the front and rear sub-cells. Inset: EL image of the WBG perovskite front cell.

3. (Evidence for the formation of TAB)

The authors indirectly demonstrated the formation of TAB in perovskite materials. While the formation of TAB as a molecule is acceptable, there is no direct evidence showing TAB formation within perovskite films during device operation. The authors should provide direct and quantitative evidence of TDB-to-TAB conversion in light-illuminated perovskite materials. Also, the authors mentioned that TAB is generated under UV illumination; however, in a solar simulator the UV portion is quite low. What fraction of TDB is converted under operando conditions?

Response: We appreciate the reviewer's comment. In response, we have provided direct and quantitative evidence that TDB is converted into TAB in light-illuminated perovskite materials under operando-relevant conditions. Specifically, by using **^{19}F NMR** as a direct analytical tool, we quantified the TDB-to-TAB conversion in perovskite films after illumination under our AM 1.5G-matched solar simulator, and found photoconversion ratios of 30.5% after 24 h and 42.0% after 72 h.

(1). To address the reviewer's concern regarding the low UV fraction in the solar simulator, we first show the spectral distribution of the xenon-lamp solar simulator used in this work **(see Fig. R36**), which matches the AM 1.5G spectrum well. Although the ultraviolet portion accounts for only ~5% of the total solar irradiance, these high-energy photons are sufficient to trigger photochemical processes {10.1038/s41560-026-01993-z}.

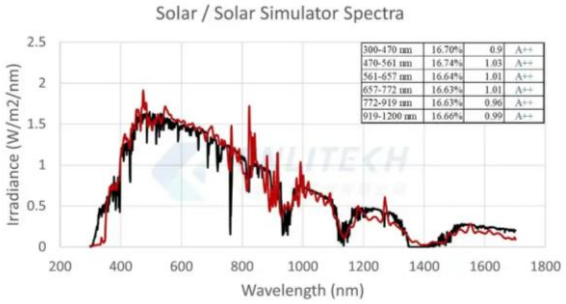

Figure. R36. Emission spectrum of the xenon-lamp solar simulator used in this study. The spectrum (red dash) was obtained from the manufacturer-provided spectral report for the xenon lamp light source configuration used in this work.

(2). We directly quantified the generated product in illuminated perovskite materials. For this analysis, a 1.8 M $MAPbI_3$ precursor solution containing 5 mol% TDB was prepared, and a total of 120 perovskite films were fabricated on 2.5 × 2.5 cm² ITO substrates. The films were then illuminated under the solar simulator, with 60 films exposed for 24 h and the remaining 60 films for 72 h. After illumination, the films were scraped from the substrates, yielding 100 mg of perovskite powder for each group, and the collected powders were dissolved in DMSO-d_6 for **^{19}F**

NMR characterization. Two distinct signals at –64.7 and –70.7 ppm were assigned to TDB and TAB, respectively. From the integrated peak areas, the TDB-to-TAB conversion ratio was determined to be 30.5% after 24 h and 42.0% after 72 h (see **Fig. R37**).

We have added Supplementary Fig. 28 in SI

We have added discussion in p. 12: "We employed ^{19}F NMR as an analytical tool to provide direct and quantitative evidence for the TDB-to-TAB conversion in perovskite film (Supplementary Fig. 28)."

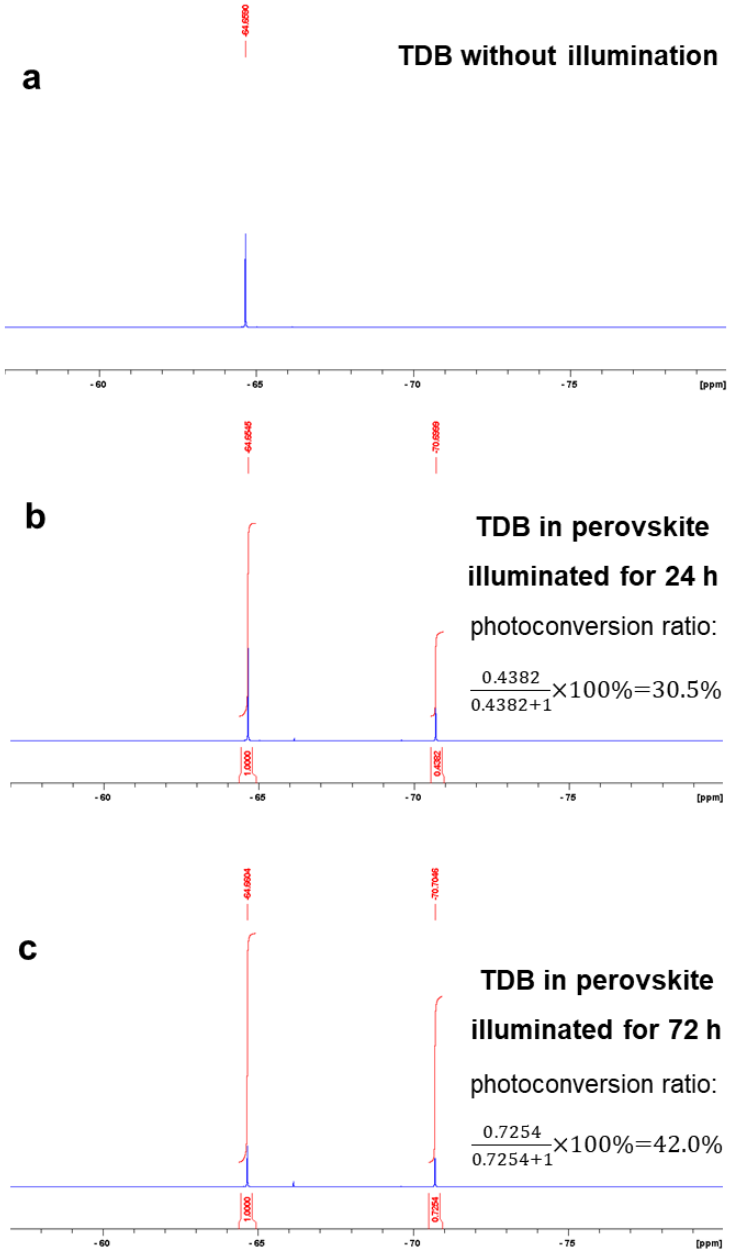

Figure R37 (Supplementary Figure. 28). Monitoring the photoconversion of TDB to TAB in perovskite films by ^{19}F NMR.

4. (Provide the binding energy of TDB)

The authors compared the binding energies of TCB and TAB. For clarity, the binding energy of TDB should also be provided, and the interactions of all three molecules should be compared.

Response: We appreciate the reviewer's comment. In the original version, TCB was discussed because it is an intermediate species in the TDB-to-TAB conversion process. However, based on the subsequent ^{19}F NMR results, we concluded that the two key species most directly relevant to the two-stage mechanism proposed in this work are TDB and TAB, corresponding to the initial state before illumination and the photo-converted state under operation, respectively. Accordingly, in the revised manuscript we have focused the comparison on these two molecules, and now provide their electrostatic potential distributions together with a comparison of their binding energies to the perovskite surface. (see **Fig. R38** and **Table R6**)

Since TCB serves as a transient intermediate rather than the dominant species governing the initial and final functional states discussed here, we believe that focusing on TDB and TAB provides a clearer and more mechanism-relevant comparison.

We have added Figure 3b-d in main text.

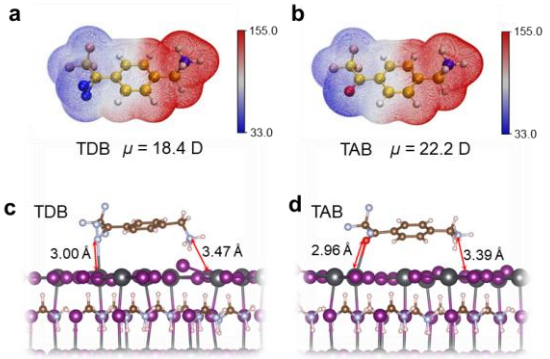

Figure R38 (Figure 3b-d) Electrostatic potential surfaces of (**a**) TDB and (**b**) TAB. Calculated adsorption models of (**c**) TDB and (**d**) TAB on the perovskite surface.

Table R6 (Supplementary Table. 4) the maximum and minimum points (φ_{max} and φ_{min}) of the electrostatic potential and adsorption energy of TAB and TDB.

molecule	φ_{max} (kcal/mol)	φ_{min}(kcal/mol)	adsorption energies
TAB	158.1	31.1	-8.2 eV
TDB	154.8	33.4	-6.9 eV

5. (Ambiguous explanation of halide segregation mechanism)

The authors state that TAB has a strong tendency to anchor at I vacancies, FA vacancies, and other defects, thereby pinning movable halide ions in the lattice. However, this explanation lacks scientific detail. Please explain this phenomenon more clearly. What is the relationship between anchoring at FA vacancies and suppressing halide-ion migration?

Response: We appreciate the reviewer's important comment. We agree that our original description of this point was not sufficiently clear. In response, we have revised this discussion to focus more specifically on **iodide vacancies and iodide interstitials** which are more directly involved in halide-ion migration than FA vacancies.

(1). In the revised manuscript, we clarified that the suppression of halide-ion migration does not arise simply from "pinning" mobile halides, but from the ability of TAB to increases the formation energies of defects, especially the iodine vacancies and iodine interstitials. The suppression of these iodide-related defects **mitigates defect-assisted carrier trapping and increases the barrier of halide ion migration**, thereby weakening carrier localization in the de-mixed state and reducing its free-energy gain. As a result, halide segregation under illumination is effectively suppressed.

We have further clarified this point in the revised main text in p.4: "The newly generated TAB with higher dipole moment exhibits stronger adsorption on the perovskite surface and increases the formation energy of iodine-related defects, thereby suppressing defect-assisted carrier trapped and halide-ion migration, consequently enhances the photo-stability of the WBG perovskite", and in p.12: "DFT calculations indicate that TAB possesses a larger dipole moment (**Fig. 3b**) and stronger adsorption on the perovskite surface than TDB (**Fig. 3c,d** and data is shown in Supplementary Table. 4), owing to its multisite anchoring mode involving electrostatic interaction through the ammonium group together with additional coordination of the carbonyl oxygen to undercoordinated Pb sites. X-ray photoelectron spectroscopy (XPS) measurements also demonstrated these results (Supplementary Fig. 29). Moreover, TAB increases the formation energies of iodine vacancies and iodine interstitials (Supplementary Fig. 30). The suppression of these iodide-related defects mitigates defect-assisted carrier trapping. Transient photocurrent (TPC) measurements (Supplementary Figure. 31) were performed on the control, TDB-treated, and TAB-treated pero-SCs. The shortest decay time observed for the TAB-treated device suggests reduced defect-assisted carrier trapping and charge accumulation[36]. Meanwhile, the reduced defect density also suppresses defect-mediated halide-ion migration[37]. To further verify the increased ion-migration barrier, we measured the temperature-dependent conductivity of the target and control samples and extracted the activation energy (E_a) for ion migration from the Arrhenius plot[38]. As shown in Supplementary Fig. 32, the target sample exhibited a higher activation energy for ion migration."

(2). Regarding FA vacancies, we agree that their role should be described more carefully. A-site cations do not directly determine the band-edge electronic states, but can indirectly influence ion dynamics and phase stability through lattice distortion, octahedral tilting, the local electrostatic environment, and defect coupling {*Science* 2022, *375*, eabj1186}. Thus, anchoring at FA-vacancy-associated defective regions is not viewed as directly blocking halide movement, but rather as stabilizing the local environment and suppressing nearby iodide-related defect formation and migration.

6. (Effect of TAB on interfaces)

The TAB molecules may influence the interfaces between perovskite and the ETL or HTL. The authors should discuss the possible interactions between TAB and each transport layer.

Response: We sincerely thank the reviewer for this insightful and important comment. We do not have direct evidence for a specific chemical interaction between TAB and the ETL or HTL, but our data support that TAB modifies the perovskite surface energetics, which is beneficial for the interfacial energy level alignment, especially at the perovskite/C_{60} interface.

We performed KPFM and UPS measurements on the surfaces of pristine perovskite films and films treated with TDB and TAB.

Both the TDB- and TAB-treated samples exhibited higher CPD values than the control (see **Fig. R39a-c**), indicating shallower work functions and a more *n*-type character at the top surface of the films according to the relation:

$$V_{\mathrm{CPD}} = (\phi_{\mathrm{tip}} - \phi_{\mathrm{sample}})/e,$$

with the TAB-treated sample showing a stronger *n*-type character than the TDB-treated one.

Based on the secondary electron cutoff and onset energy obtained from UPS (see **Fig. R39d**), together with the optical bandgap of 1.88 eV derived from UV–vis spectroscopy, we constructed the energy-level diagrams of the corresponding devices (see **Fig. R39e**). The results reveal that both TDB and TAB reduce the energy offset between the CBM of perovskite and the LUMO level of C_{60}, thereby improving the energy-level alignment at the perovskite/C_{60} interface, facilitating electron extraction and transport, and reducing interfacial energy losses. Notably, the modulation induced by TAB is more pronounced, which is likely associated with the stronger interfacial dipole effect generated by this polar molecule.

We have added Supplementary Fig. 21 in SI.

We have added Supplementary Fig. 22 in SI.

We have added discussion: "We performed Kelvin probe force microscopy (KPFM) and ultraviolet photoelectron spectroscopy (UPS) measurements (Supplementary Figs. 21 and 22) on the surfaces of pristine perovskite films and films treated with TDB. The TDB-treated film exhibited lower contact potential difference (CPD) values than the control, indicating shallower work functions and a more *n*-type character at the top surface. Based on the UPS results, we constructed the energy-level diagrams of the corresponding devices (Fig. 2h). The results reveal that TDB treatment reduce the energy offset between the perovskite conduction band minimum (CBM) and C_{60} LUMO, thereby optimizing the energy-level alignment at the perovskite/C_{60} interface, facilitating electron extraction and reducing interfacial energy losses. This effect may originate from interfacial dipoles introduced by TDB[31]"

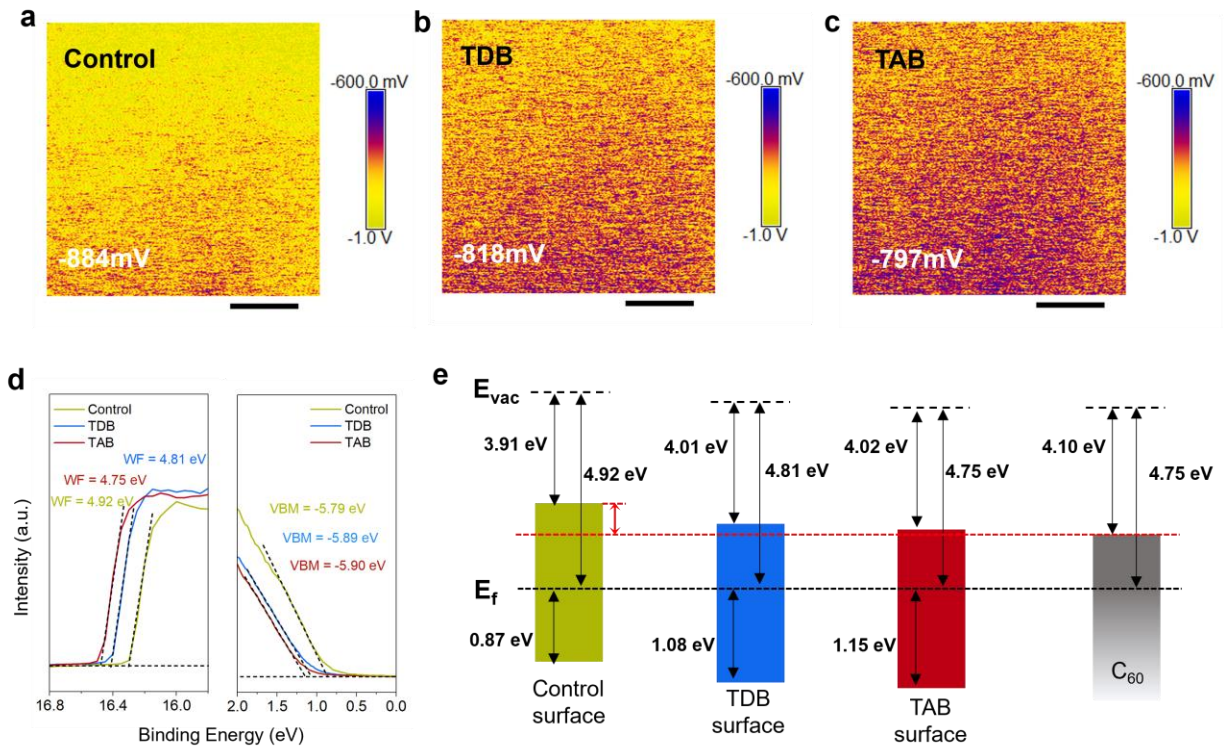

Figure. R39 (Supplementary Figures. 21 and 22) a-c KPFM surface potential maps of the top surfaces of perovskite films with different additive treatments. **d**, UPS spectra of the top surfaces of perovskite films with different additive treatments. **e**, Energy level alignment diagrams for the top surfaces of perovskite films with different additive treatments and C_{60}. The energy offset between the CBM of the control perovskite surface and the LUMO of C_{60} is 0.36 eV, which is markedly reduced to 0.15 eV after TDB treatment and further to 0.08 eV after TAB treatment.

7. (Stability of the tandem cell)

The authors provide stability data only under mild ISOS-L-1 conditions. For real applications, stability under harsher conditions (e.g., 85 °C/85% RH) is needed. Also, the MPPT duration of 300 s is not sufficient to demonstrate long-term stability.

Response: We sincerely thank the reviewer for this important comment. In response, we have strengthened the stability evaluation in the revised manuscript by **adding accelerated-aging data under harsher conditions** and by **extending the duration of continuous MPP tracking**. Besides, we discuss **the intrinsic stability potential** of perovskite–organic TSCs in view of the complementary properties of the WBG perovskite front cell and the NBG organic rear cell.

(1). We evaluated the thermal stability of encapsulated perovskite–organic TSCs under accelerated aging at 85 °C, following the ISOS-D-2 protocol. Under these standardized dark thermal stress conditions, the encapsulated tandem devices maintained over 80% of their initial performance for more than 600 h (T_{80} > 600 h), demonstrating the thermal robustness of this tandem architecture. (see **Fig. R40**)

We have added the discussion in the revised manuscript on p.16: "Under accelerated aging at 85 °C (ISOS-D-2), the encapsulated TSCs maintained over 80% of their initial performance after 600 h, demonstrating the thermal robustness of the tandem architecture (**Fig. 4h**)."

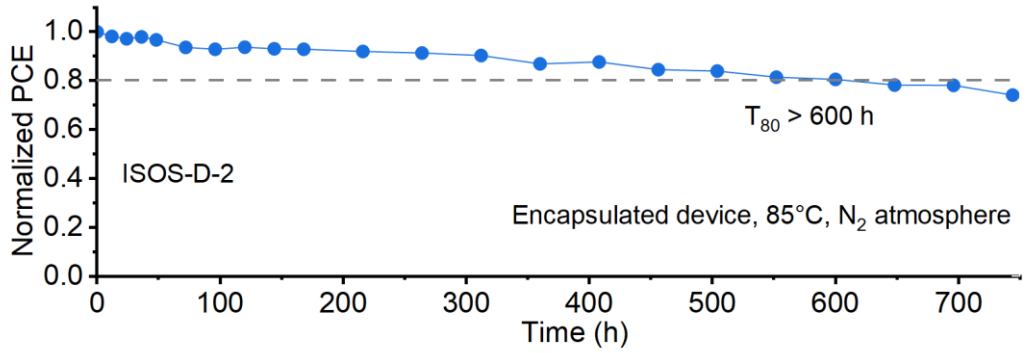

Figure R40. (Figure 4h). Operational stability of encapsulated perovskite–organic TSCs under accelerated aging at 85 °C, following the ISOS-D-2 protocol.

(2). As suggested by the reviewer, we extended the continuous MPPT duration of the encapsulated perovskite–organic TSCs far beyond the originally presented 300 s interval. The data show that the devices retained about 90% of their initial performance after approximately 672 h of continuous MPP tracking under illumination (see **Fig. R41**). To further quantify the long-term degradation behavior, we fitted the data using a biexponential empirical model, which has been widely adopted to describe non-linear performance decay in perovskite-based photovoltaic

devices {*Science* 2022, *377*, 307–310}. Based on this empirical fit under the ISOS-L-1 protocol, the devices are projected to retain over 85% of their initial performance after 1000 h of continuous MPP tracking.

We have also added the discussion in the revised manuscript on p. 15: "The TSCs maintained 90% of their initial efficiency after about 672 h of continuous illumination. By fitting the degradation data with a biexponential decay model ($R^2 > 0.95$), we extrapolated a projected T_{85} exceeding 1000 h (**Fig. 4g**), demonstrating strong stability under operational conditions."

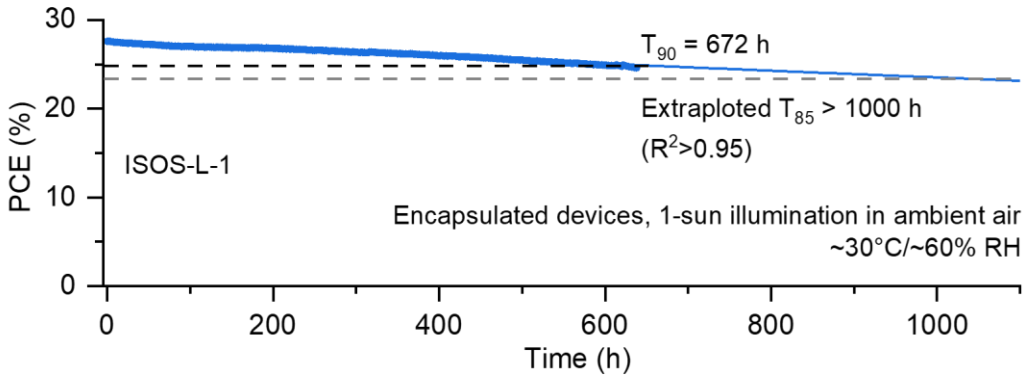

Figure R41. (Figure 4g). Long-term MPP tracking of the encapsulated perovskite–organic TSCs under simulated 1-sun illumination in ambient air without temperature control.

(3). We supplemented the manuscript with experiments supporting the intrinsic stability potential of perovskite–organic TSCs, especially the complementary properties of the WBG perovskite front cell and NBG organic rear cell.

Firstly, the WBG perovskite front cell can effectively filter ultraviolet light and a substantial fraction of the visible spectrum, thereby shielding the NBG organic rear cell from high-energy-photon-induced degradation, which is among the most detrimental stress factors for organic solar cells (OSCs). {*J. Mater. Chem. A* 2021, *9*, 19778–19787}, {*Nature* 2022, *604*, 280–286}. We placed a quartz substrate coated with a WBG perovskite film (encapsulated) in front of an encapsulated OSC under ambient air conditions, simulating the spectral filtering scenario in the TSCs. Under continuous MPP tracking, the filtered organic device maintained over 95% of its initial output power for over 1100 h ($T_{95} > 1100$ h). In contrast, the OSCs without WBG perovskite filtering degraded to 84% of its initial efficiency after 550 h (see **Fig. R42**).

We have added Supplementary Fig. 41 in SI.

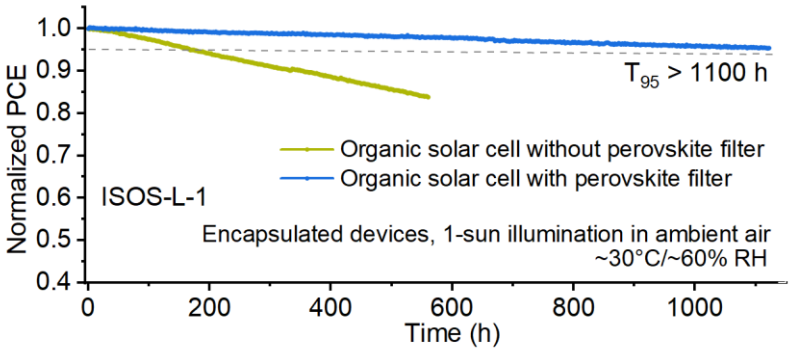

Figure R42. (Supplementary Figure. 41) Long-term MPP tracking of the encapsulated OSC without and with a WBG perovskite filter under simulated 1-sun illumination in ambient air.

Secondly, we investigated the operational stability advantage of perovskite–organic TSCs due to the hydrophobic properties of the organic rear cell. The ~120 nm-thick organic active layer is intrinsically hydrophobic and acts as an additional barrier shielding the perovskite front cell from moisture—a detrimental stress factor that can rapidly trigger perovskite decomposition. Accordingly, we conducted accelerated aging tests under 85% relative humidity (RH) in ambient air. When comparing unencapsulated WBG perovskite single-junction devices with unencapsulated perovskite–organic TSCs, the unencapsulated WBG perovskite single-junction devices exhibited a rapid performance decline within the first 12 h. In contrast, the unencapsulated perovskite–organic TSCs showed markedly improved storage stability under the same high-humidity conditions (see **Fig. R43**).

We have added Supplementary Fig. 42 in SI.

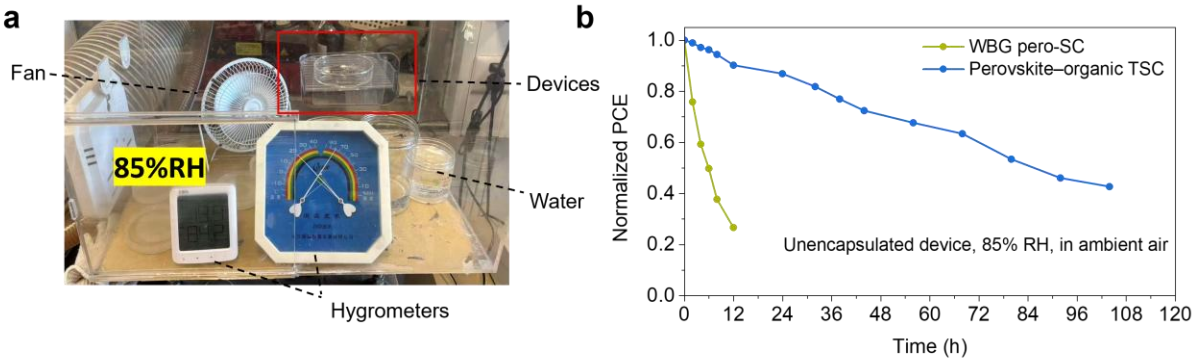

Figure R43. (Supplementary Figure. 42) a, Photograph of the humidity-controlled setup. There are devices, water, hygrometers and fan in the storage box. **b**, Operational stability of unencapsulated WBG perovskite-SCs and unencapsulated perovskite–organic TSCs under high-humidity accelerated aging condition (85% RH in ambient air).

Within only 12 h, the perovskite absorber visibly transformed from the black perovskite phase to yellow PbI_2 under the high-humidity conditions, concurrently, the Ag electrode exhibited obvious degradation. In contrast, the perovskite absorber in the unencapsulated perovskite–organic TSCs retained its black phase under the same high-humidity conditions (see **Fig. R44**).

We have added Supplementary Fig. 43 in SI.

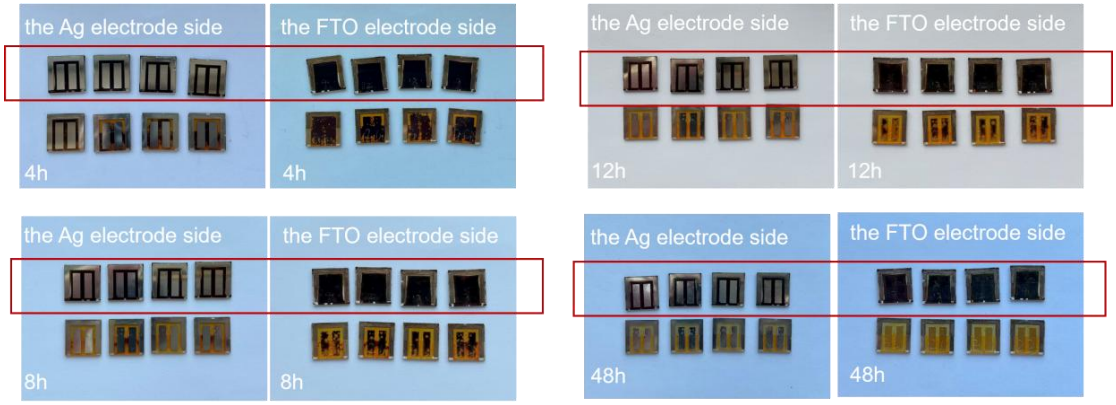

Figure R44. (**Supplementary Figure. 43**) Photograph of devices under high-humidity accelerated aging condition (85% RH in ambient air). The perovskite–organic TSCs are enclosed in the red box in the photograph, with the WBG perovskite-SCs located below.

8. (9 mm² cell size)

Many recent papers have reported module-scale or large-area devices. Although the >28% efficiency is high, the cell area is only ~9 mm². To demonstrate practical applicability, the authors are encouraged to present tandem-cell performance on a larger area.

Response: We sincerely thank the reviewer for this valuable suggestion. In fact, we have been making continuous efforts to improve the efficiency of large-area perovskite–organic TSCs. Benefiting from the optimization of the WBG perovskite front cell, we achieved a PCE of 28.02% on a 1 cm^2 perovskite–organic TSC. This result further supports the potential of perovskite–organic TSCs for large-area fabrication

We have added Supplementary Fig. 45 in SI.

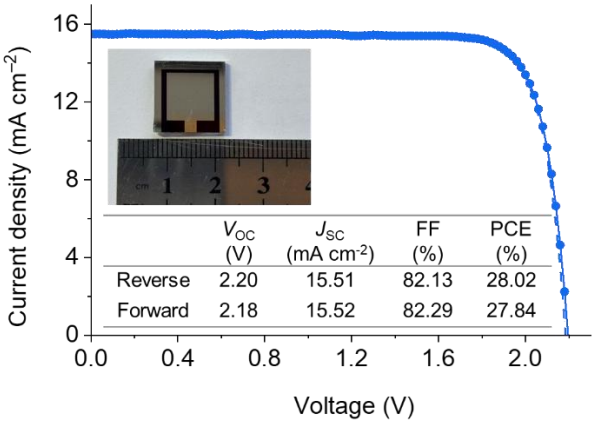

Figure R45 (Supplementary Fig. 45). *J–V* curve and photograph of the champion 1-cm^2 perovskite–organic TSC.

Table R7. the V_{oc}, J_{sc}, FF and PCE values of the peroskite–organic TSC with device area of 1.001 cm^2, under the illumination of AM1.5G, 100 mW cm^{-2}.

	V_{oc} (V)	J_{sc} (mA cm^{-2})	FF (%)	PCE (%)
Reverse	2.20	15.51	82.13	28.02
Forward	2.18	15.52	82.29	27.84

9. (Typo)

- Misuse of "TBD" instead of TDB on page 14

- In Fig. 3i, please add a legend ("target" and "control")

- "addictive" → additive on page 7

Response: We sincerely thank the reviewer for these careful and helpful comments.

We have corrected the misuse of "TBD" to "TDB" on page 14 in the revised manuscript.

We have also added the legend ("target" and "control") to **Fig. 3i** for improved clarity.

The typographical error "addictive" has been corrected to "additive" on page 7.